ESTIMATING THE PARAMETERS OF FITZHUGH-NAGUMO NEURONS FROM NEURAL SPIKING DATA

A THESIS SUBMITTED TO
THE GRADUATE SCHOOL OF NATURAL AND APPLIED SCIENCES
OF
ATILIM UNIVERSITY

BY

LAILA ABOSHARB

IN PARTIAL FULFILLMENT OF THE REQUIREMENTS
FOR
THE DEGREE OF DOCTOR OF PHILOSOPHY
IN
MODELING AND DESIGN OF ENGINEERING SYSTEM,

JANUARY 2020

Approval of the Graduate School of Natural and Applied Sciences, Atilim University.

_____

Prof. Dr. Ali KARA

Director

I certify that this thesis satisfies all the requirements as a thesis for the degree of **Doctor of Philosophy in Modeling and Design of Engineering System, Atilim University**.

_____

Assoc. Prof. Dr. Ender KESKİNKILIÇ

Head of Department

This is to certify that we have read the thesis Estimating the Parameters of Fitzhugh-Nagumo Neurons from Neural Spiking Data submitted by LAILA ABOSHARB and that in our opinion it is fully adequate, in scope and quality, as a thesis for the degree of Doctor of Philosophy.

_____

Assoc. Prof. Dr. R. Özgür DORUK

Supervisor

Examining Committee Members:

Prof. Dr. Fahd JARAD
Dept. of Mathematics, Çankaya University _____

Assoc. Prof. Dr. R. Özgür DORUK
Dept. of EEE, Atılım University _____

Asst. Prof. Dr. Hakan TORA
Dept. of EEE, Atılım University _____

Asst. Prof. Dr. Özgür ERGÜL
Dept. of EEE, Atılım University _____

Asst. Prof. Dr. Dumitru BALEANU
Dept. of Mathematics, Çankaya University _____

Date: 17.1.2020

I declare and guarantee that all data, knowledge and information in this document has been obtained, processed and presented in accordance with academic rules and ethical conduct. Based on these rules and conduct, I have fully cited and referenced all material and results that are not original to this work.

Name, Last Name : LAILA ABOSHARB

Signature :

ABSTRACT

Estimating the Parameters of Fitzhugh-Nagumo Neurons from Neural Spiking Data

ABOSHARB, Laila

Ph.D., Department of Modeling and Design of Engineering System,

Supervisor : Assoc. Prof. Dr. R. Özgür DORUK

January 2020, 60 pages

In this thesis, we attempt to estimate the parameters of a single Fitzhugh-Nagumo neuron based on the neural spiking data. In this model, the input is an electric current serves as the stimulus while the output is considered to be the firing rate of neural spiking. The difference from the conventional system identification techniques is that no continuous variation of the response (the membrane potential or firing rate) is available. Instead, the data consists of the peak timings of action potentials called as spikes. One major property of these is that they are generated as a result of stochastic processes (ion channel stochasticity). Thanks to the arrival processes in statistics one can implement likelihood functions to estimate those parameters. In the simulation frame work one needs either to simulate the neural spiking or use a set of spike trains obtained from realistic data. For algorithmic testing of the methodologies developed in this research an inhomogeneous Poisson process is simulated using the firing rate response of a Fitzhugh-Nagumo model with known nominal parameters. The firing rate response is obtained from a predefined stimulus which is in Fourier series form with superimposed cosines. The simulations are repeated multiple times with different stimulus phases (phases of cosine functions in Fourier series) to obtain enough statistical content. The simulated stimulus-response data is then provided to the inhomogeneous Poisson likelihood functions (derived under Local Bernoulli approxi-

mation) to obtain an estimate of the neuron model parameters. The mean estimated values are presented as tables and their statistical analysis are presented graphically. The graphs present the variations of the standard deviations of the estimates against different values of stimulus component sizes, base frequency, amplitude and number of samples. In addition, in order to validate the performance of the methodologies developed in this thesis a realistic stimulus/response data is obtained from external sources (H1 neurons of blowflies) and the algorithms are applied. Here the vision system of the flies are stimulated by a 20 minute white noise stimulus and the neural spikes are collected. It is also convenient to test the algorithm with a different set of data other than Fouries series based ones. The computational environment is based on MATLAB and its constrained optimization routine `fmincon` is used in the likelihood estimation.

Keywords: Neuron modeling, Fitzhugh-Nagumo model, In-homogeneous Poisson processes, Neural spiking, Maximum likelihood estimation

ÖZ

Sinirsel Ateşleme Verisinden Fitzhugh-Nagumo Nöron Modelinin Parametre Kestirimi

ABOSHARB, Laila

Doktora, Mühendislik Sistemlerinin Modellenmesi ve Tasarımı (Ana Çalışma Konusu: Elektrik ve Elektronik Mühendisliği)

Tez Yöneticisi : Doç. Dr. R. Özgür DORUK

Ocak 2020, 60 sayfa

Bu tezde Fitzhugh-Nagumo sinir hücresi modellerinin parametrelerinin sinirsel ateşleme verisinden kestirilebilmesine yönelik bir araştırma yapılmaktadır. Söz konusu modelde girdi bir elektrik akımı olup uyaranı temsil etmekte olup çıktı olarak ise ateşleme hızı modelden alınmaktadır. Konvansiyonel sistem tanılama yöntemlerinde karşılaşılan durumlardan farklı olarak elde edilen ölçümlerde sürekli örneklenmiş bir veri (zar potansiyeli ya da ateşleme hızı) söz konusu değildir. Tam tersine, sadece aksiyon potansiyeli zamanlarından oluşan ayrık bir veri toplanmaktadır. Diğer önemli bir özellik ise bu verilerin iyon kanallarının istatistiksel süreçleri nedeniyle rastgele oluşudur. Varış rastgele süreçlerinin istatistiksel tanımlanabilirlikleri sayesinde model parametrelerinin kestirimi için olabilirlik fonksiyonlarının tanımı yapılabilmektedir. Benzetimler sırasında ya sinirsel ateşleme zamanları modelin çözümü yoluyla elde edilmeli ya da bir deneyden gerçekçi veri toplanmalıdır. Algoritma sınanması amacıyla birinci yöntem tercih edilebilir. Burada parametreleri bilinen modelden elde edilen ateşleme hızı verisi, homojen olmayan Poisson süreci benzetimi yapılarak sinirsel ateşleme verisine dönüştürülür. Söz konusu benzetimlerde önceden tanımlanmış bir uyaran profiline gereksinim vardır. Bu çalışmada Fourier serisi biçiminde tanımlanmış uyaran

profilleri söz konusu olmaktadır. Ayrıca istatistiksel yeterlilik sağlanması için benzetimler çok defa tekrarlanmaktadır. Bu işlem sırasında faz açıları rastgele atanarak benzetimlerin bağımsızlıkları garanti altına alınmıştır. Benzetimlerden elde edilen uyaran/cevap verisi yerel Bernoulli süreçlerinden türetilmiş homojen olmayan Poisson olabilirlik fonksiyonları üzerinden nöron parametrelerinin en yüksek olabilirlik kestirimi yapılmaktadır. Kestirimi yapılan parametrelerin ortalama değerleri tablolar halinde, istatistiksel özelliklerinin değişimi de grafikler halinde sunulmaktadır. Söz konusu grafikler kestirimin standart sapmalarının Fourier serisi uyaranın alt eleman sayısı, taban frekansı, genliği ve örnekleme (tekrarlanmış benzetim) sayısına karşın değişimini incelemektedir. Tüm bunların yanı sıra, geliştirilen yaklaşımların performansını inceleyebilmek için dış kaynaklardan gerçekçi uyaran/cevap verisi (gök sineklerinin H1 görme sisteminden alınmaktadır) alınmış ve geliştirilen algoritmalar bu verilerle denenmiştir. Burada sineklerin görme sistemleri renksiz gürültü biçiminde uyaranlarla 20 dakika boyunca uyarılmış ve sinirsel ateşleme verileri toplanmıştır. Bu deneme aynı zamanda Fourier serisi dışında bir uyaran ile çalışabilme olanağı da sunmuştur. Bu açıdan algoritmaların daha genel bir testine de olanak sağlamıştır. Çalışmada kullanılan hesaplama ortamı MATLAB olup, en iyileme (optimizasyon) kütüphanesinde bulunan `fmincon` betiği olabilirlik kestiriminde kullanılmaktadır.

Anahtar Kelimeler: Nöron Modellemesi, Fitzhugh-Nagumo Modeli, Homojen Olmayan Poisson Süreci, Sinirsel Ateşleme, En İyi Olabilirlik Kestirimi

To Libya

One day you will enjoy safety and stability and you will be the most wonderful place in the world, this is a promise from God only patience, my country.

ACKNOWLEDGMENTS

First and foremost, praises and thanks to the **God, the Almighty,** for His showers of blessings throughout my research work to complete the research successfully.

I would like to acknowledge my indebtedness and render my warmest thanks to my supervisor **Assoc. Prof. Dr. R. Özgür Doruk**, who made this work possible. His friendly guidance and expert advice have been invaluable throughout all stages of the work.

I am extending my thanks to **Prof. Dr. Fahd JARAD** and **Asst. Prof. Dr. Hakan TORA,** They generously gave their time to offer me valuable comments toward improving my work.

I am very much thankful to **members** of the jury for devoting time and interest to reading this report.

I am extremely grateful to **my parents** for their love, prayers, caring and sacrifices for educating and preparing me for my future.

I express my special thanks to my husband **Salem Alaradawi**, for his love, understanding, prayers and continuing support to complete this research work.

I want to say for my love children**Yakeen, Omar, Yumna** and **Abdulaziz**, who provide unending inspiration, every thing was because of you in my life and all what I did and will do for you.

I would like to express my deep gratitude to **my sisters** and **my brothers** for their endless and continuous encourage and support throughout the years study.

Finally, my thanks go to all **my friends** who have supported me to complete the research work directly or indirectly. Thank for everyone supported me, even if this support was a word.

TABLE OF CONTENTS

LIST OF TABLES

TABLES

LIST OF FIGURES

FIGURES

LIST OF SYMBOLS

$r(t)$	:	the firing rate
V	:	the membrane potential
t_k	:	the spike instances
θ	:	the estimated parameters
(a, b, c, d)	:	the FHN model parameters
F	:	the maximum firing rate
σ	:	the standard deviation
I	:	the stimulus input
A	:	the amplitude
ϕ	:	the phase of stimulus
f_0	:	the base frequency of stimulus

CHAPTER 1

INTRODUCTION

Mathematical simulations concerning biological neurons attract a lot of attention among scholars these days and go as far back as five decades within the field of neuroscience. These models may be grouped in different ways – among them, compartmental, cascade, and black box. The first group is for one or more compartments - the Hodgkin–Huxley [2] being the example of one-compartment, and the reduced version [3] well represented by Fitzhugh–Nagumo models [4] and, hence, falling within the same category. It is fair to state that [5] represents multi-compartmental simulations – once again, all regarded as rather complex and, yet, realistic biophysical models. In case such biophysical properties are not the main issue, then the cascade style comes into the fore and may be developed by combining linear filters with non-linearity to represent computational processes within the network and mostly addressed in [6, 7] referring to visual systems.

System parameter estimation a point of intrigued and investigate in a few decades, in specific, the recognizable proof of neuron models has been the matter of a few references. [8] recognize the parameters of the HH show utilizing reenacting toughening, hereditary calculations, and differential advancement procedures. [9] propose a demonstrate reference versatile strategy to appraise the parameters of the HH neuron demonstrate. [10, 11] create versatile spectators for evaluating the state and parameters of a family of neural models; in this case, the creators propose a arrange change that grants modifying the neural models within the canonical versatile eyewitness shape. Deng et al. [12] display a strategy combining the unscented Kalman channel [13] and a synchronization-based strategy for evaluating the parameters of the FHN and HR models. [14] compare two strategies for estimating the parameters of the HR neuron model, to be specific, a synchronization-based parameter estimation [15] and

an adaptive observer. These two techniques use the synchronization error between the neuron model and the data recorded from the genuine neuron. On the other hand, [16, 17] propose distinguishing proof procedures centered within the parameter estimation of the FHN show. In arrange to assess this model, [16] utilize the least squares algorithm calculation and the Daubechies Wavelet denoising procedure [18]. This method,This method, which will be called in the sequel (DBIM) the derivative based identification method, , employs the first and second time derivatives of the membrane potential; moreover, the input current stimulus must be continuously differentiable, a fact that is not fulfilled by signals like pulses, which are commonly employed for exciting neurons. The method employed by [19, 20] relies on statistical tools for estimating the noise.

Such models are not considered complicated to the extent of compartmental ones, though there is a certain degree of dynamical attributes. Speaking of black box models, they are often focused on the ability to process signals from neurons. A good number of these models have possess statistics related to likelihood distribution for the response against a stimulus. For examples, see [21, 22] Also, in [23] there is a comprehensive review of neuron simulation.

The literature contains many other methods for simulation and, according to [23], signal processing of neurons is of stochastic nature, with a degree of randomness owed to such stochasticity within the ion channels and synaptic operations. More lately, [24, 25] focus on the simulation of channel noise. Other works address the movement of ions within the channels which produces electromagnetic fields, possibly leading to coupling due to modulation of membrane potential within the post-synaptic neurons [26, 27]. Such events, too, are of stochastic nature and give rise to information processing of a similar characteristic. The research in [25] iterates that powerful magnetic fields due to electrical systems within the heart are of major impact in the organ's functioning. Any contact with such fields from the outside can generate exogenous malfunctions within the electrical operations of neurons [28, 29], causing unanticipated dynamical reactions to occur, for instance double coherent resonance [30].

Applying active or stationary neural networks to simulate biological ones is also addressed within the literature. Certain attempts, such as [31] and [32] concentrated on the focus on using stationary feed forward neural networks for simulating the auditory cortex. These static networks do not account for the time-dependency of the process

within biological neurons – such as action potentials, refractory regions, and others. For this reason, active and repetitive neural networks can, instead be applied to define signal processing attributes – for instance, [33, 34] carried out this process using membrane potentials as the active variables.

Continuous time recurrent neural networks [35] is equipped with self-initiating and/or self-preventing joints equal to a case of dissection analysis where synaptic bonds are shaped between segments within one neuron (for instance, dendrites and axon). Such dissection joints may obtain the signal transduction in the event of neurodegenerative diseases [36, 37]. as well as change or adjust the active elements within neurons [38, 39].

In [40, 41] the authors claim that neural spiking scenarios related to sensory neurons, to a large extent, follow inconsistent Poisson patterns. Since such inconsistent point processes have very comprehensive likelihood mass functions, as stated in [42], a practical method to determine the parameters is maximum probability [43, 44].

Neuron parameter determination is popular among both theoretics and computational neuroscience studies. Once the firing rate is regarded as calculable, we may use the standard least square approach [45], coordination [46], and adaptive Lyapunov +s ynchronization-based approaches for the purpose [15]. Nonetheless, for the present study, the data gathered is not homogeneous and there is no detail related to amplitude/rate. As a consequence, the techniques proposed in the citations may not be used as they are. Lately, some efforts have been made to make use of coordination or synchronization techniques for spiking neurons. The task is mainly about the alignment of two neural spiking events through the reduction of inter spiking intervals (ISI). To provide an example, [47] makes use of spike synchrony monitoring approach [48] by reducing the vanRossum distance [49] from one spike train to the next. The primary factor within this technique is the need for a medium [50] to calculate the van Rossum distance; thereby adding to the level of complexity and, as such, exclusion from our study here. Instead, we introduce a model-based mechanism geared toward assessing the parameters of a firing rate-based single neuron model. In brief, these are the steps to be taken here:

1. Considering a predetermined stimulus (Fourier series and others),we simulate the model with actual parameters within a specific duration to collect the exact

profile of the firing rate.

2. By means of modeling the inconsistent Poisson patterns, we gain the anticipated spiking profile in the next step.

3. Later, we repeat the above process numerous times for satisfactory statistical data.

4. By applying the highest probability approach, the determined spike trains are applied to collect the related model parameters.

5. Various stimuli of alternative configurations are then studied to collect enough information to be used for comparative analyses.

Related other investigations appear in the available discourse. See [39, 42], where a feed forward dynamical static neural network is trained based on data pertaining to neural spiking. Here, in contrast, the focus will be on a more basic, yet similarly active and dynamical, time-based framework – hence, establishing another new contribution to the already existing body of work concerning computational neuroscience.

CHAPTER 2

NEURONS AND TRANSMISSION OF NEURAL INFORMATION

The neural system may as well be regarded as the worldwide web of our body as transmits various forms of messages to different spots within. Being primarily of biological nature, such operations will make one question if math specialists began to investigate their workings; indeed, applied math experts receive training for modeling cases in actual settings within physics, chemistry, electro-technics and biology. Such activities matter greatly since the appropriate framework can assist experts from all fields to work together. To illustrate, we may simulate nerve pulses using waves. In this regard, the pattern introduced by Hodgkin and Huxley (HH) had its own intricacies, and measuring waves proved challenging. Contrarily, one may argue that the Fitzhugh-Nagumo (FN) pattern rather makes the process easier while offering a satisfactory definition for nerve signals.

2.1 The Neuron

Similar to other forms of cells, neurons comprise a makeup otherwise known as soma, where the core or nucleus is located. Neurons are bound to generate a significant amount of proteins, which are again arranged in the soma itself. Different formations, such as ad-junctions and projections branch out of the body section of the cell and comprise numerous tiny extensions or dendrites, along with a different and often larger formation – that is, the axon. Obviously, a majority of human thinking includes processes taking place throughout the nerves and mainly the brain itself. Our nervous

system houses cells in their billions, among which neurons are of particular importance and number 100 billion on average. Commonly, neurons share the same cell from with others, along with a number of specific formations distinguishing them. The main body is known as soma and includes a core or nucleus with all the genetic content as chromosomes. There are numerous branches extending from neurons, referred to as dendrites, with a surface area mostly taking in all chemical messages from nerve cells One more section. [51]

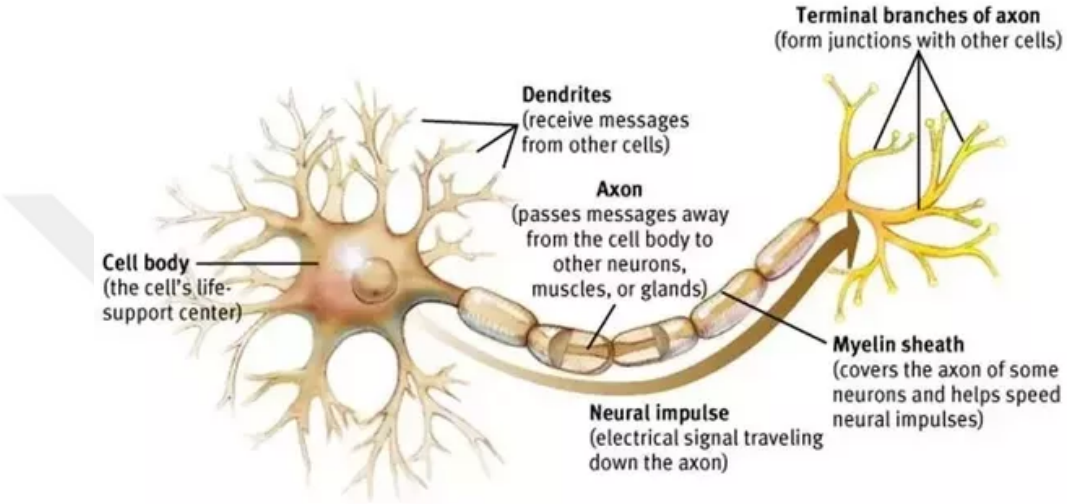

Figure 2.1: Structure of Neuron

The axon is among these branches and slightly different since, despite being hard to tell apart from dendrites in certain cells, it may be identified by its length in other cases. The axon sends out electro-chemical pulses across very long extensions, sometimes a distance of three feet - that is in case of the nerve cells stretching from the spine all the way to our toes.

In other more extended axons, a layer of myelin covers them comprising a set of fatty cells extended over the axon in multiple rounds and, thus, resembling a pendant with sausage-like components hanging from it. This sheath is a form of protection in the same manner electrical wires are covered with plastic casing.

The end of the axon - known as bouton, synaptic knob, and foot – changes the electro-chemical pulses to merely a chemical message to be passed on to neighboring nerve cell.

2.1.1 Action Potential

Once any chemical compound touches a neuron, the ions shift in balance, thereby changing the electrical charge on the inner and outer parts of the nerve. Upon arriving at a certain limit, the impact travels through the cell toward the axon, where it generates the action potential – in other words, the speedy movement of ions.
On the axon are numerous tiny membranes or ion channels which, upon the arrival of the electric pulse at the bottom of the axon, release the positive ions into the axon and cause a shift in the electrical charge within and outside. In turn, this results in a similar reaction in the neighboring set of channels whereas the rest send back out the positively charge ions. The process continues along the length of the axon.

Other related processes taking place in nerve cells are as in the following

1. Stimulus initiates a quick shift of voltage or action potential. In patch-clamp mode, enough charge has to be applied to increase the voltage over the threshold and trigger membrane depolarization.

2. Such depolarization occurs upon a sharp increase in membrane potential opening of sodium channels in the cell, causing the release of vast amounts of sodium ions.

3. Membrane Repolarization is caused by quick sodium channel inactivation along with a major potassium ion discharge due to the activated potassium channels.

4. Hyperpolarization is caused by reduced membrane potential due to a rush of potassium ions and a shut-down in potassium channels.

5. Resting state occurs once the membrane potential resumes the normal and inactive or resting-state voltage.

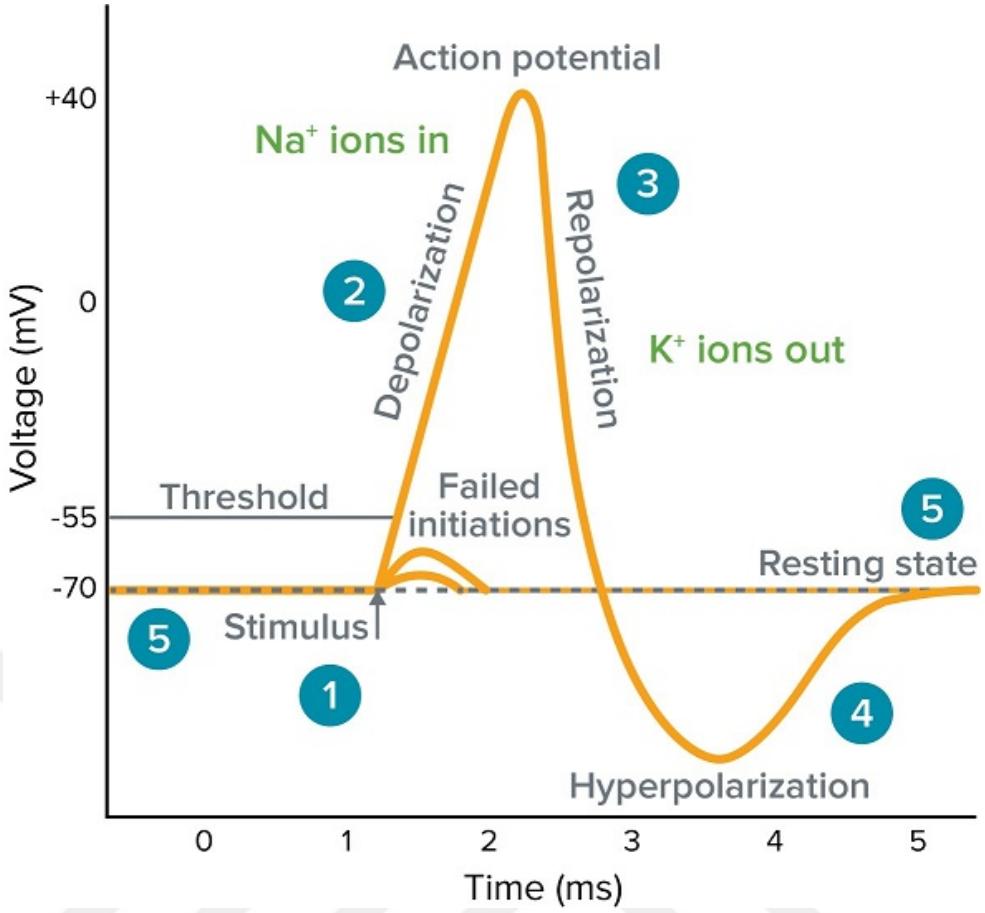

Figure 2.2: Action Potential

2.2 Spiking Neuron Network (SNN)

Spiking neural networks (SNNs) are part of the third version of NN models and add to the degree of reality in related simulation processes. Apart from neuron-related and synaptic state, these networks take into account the time factor, with the main concept being that the neurons are not triggered in every round of propagation – unlike conventional multi-layer perception models; instead, they fire merely once a membrane potential, in comparison to its relative membrane electrical charge, achieves a certain degree (vague original sentence. Once it releases a pulse, the neuron creates a signal to move on to other nerve cells, thereby reducing or spiking their related potentials accordingly.

Within SNNs, the current activation level – designed in the form of differentials- may

be commonly regarded as the state of the neuron along with arriving spikes that increase its value, and finally the firing or decaying in time. There are numerous ways to codify this process and explain the exit spike train in the form of an actual-value by depending upon spike frequency or, alternatively, the period between two spikes in order to turn the data into codes.

2.3 Spike Train

A spike train in plain terms combines a series of spikes and silences known as inter-spike intervals or ISI. One common approach to view them is in the form of a digital series of data: 1 for a spike, and 0 for no spike. To illustrate, an encoded spike train formation may resemble 001111101101, where the initial 2 0s stand for the delay between the stimulus introduction and the initial spike generated. One may trigger a spike train by means of physical sensory stimulus like vision, touch, smell or sound; another way is to apply abstract ways like perception and cognitive stimulus through, for instance, triggering a memory. Commonly the length and form of spike trains rely on the degree and length of the stimuli, and may continue until such stimuli fades. Yet, certain nerve cells possess electrical features of their own by which they can produce constant reaction toward even brief stimuli.
In such events, larger stimulus intensities can cause lengthier spike trains. In all, continuous stimulus may create spike trains and, yet, certain neurons may simply need very short stimuli to generate extended spike trains.

2.4 Neural Firing Rate

Typically, a pattern to create spikes is by the Poisson point approach to produce action potentials as a function of an underlying rate function. Such firing rate is subject to behavior, stimuli, neighboring neurons, spiking background, or numerous other elements. As a result, it helps to assess this rate based on the spike train of a neuron so that one may compare the outcome under test settings.
We may assess the firing rate using one spike train or an ensemble average of spike train formed within similar settings and in the same way as a repetitive stimulation,

repetitive motion, and so on.

2.4.1 Estimating the Firing Rate

Spikes may be estimated as per second or firing rate. With numerous tests, one may estimate the average number of spikes within a period and divide the figure by that time window to find out the exact number each second for a certain time instant.
The above method, of course, is most common and simplest to estimate firing rate, with the disadvantage of rate relying on bin-size – the bigger the bin, it is likely to eliminate meaningful firing rate modeling; whereas the smaller the bin, it is likely to preserve meaningful firing rate modeling and yet not properly eliminate changes caused by noise. In this way, the choice of bin-size resembles assessing the speed at which we anticipate the underlying firing rate function to fluctuate. Also, let us not forget the numerous hypotheses related to this operation, namely the presence of the underlying rate itself as well as related timescales of change.
The firing rate relates to how many spikes are formed by a neuron within a given unit of time. Temporal encoding can compress information more compared to rate-encoding. Likewise, the former also takes place in our brain as well thanks to our power to quickly recognize patterns. certain studies have proposed that the operation may be defined merely by the action potential timing for encoding because analogue pattern matching can be accomplished within a time scale in many milliseconds, not to mention that biological neurons tend to oscillate at just about 100 Hz. Such observations have been made in visual pattern analysis and pattern classification on macaque monkeys at a time response of only 2030ms. Given neuron firing rates of less than 100Hz, experts commonly encode analogue variables based on firing rates – which is a questionable practice when it comes to pattern recognition.

2.5 Simulation of Neural Spiking

Spike times represent continuous variables; henceforth, the likelihood of any spike to take place at a precise point in time is regarded as almost non-existent. To achieve otherwise, one should inquire the likelihood of a spike appearing during a certain in-

terval, say that between times t and $t + \Delta t$. In case of lesser Δt values, this likelihood can be in relation to the actual size of the interval. A likewise ratio is true in case of any given continuous stochastic variable z. The potential that z receives a value between z and $z + \Delta z$, for lesser Δz values – mainly as $\Delta z0$) – equals $p[z]\Delta z$, in which $p[z]$ is regarded as probability density [52].

The firing rate $r(t)$ shows the likelihood of releasing one spike in a short interval around the time t; yet, commonly $r(t)$ does not provide enough data to forecast the likelihood of an entire spike sequence or sequences. To illustrate, the chance for two spikes appearing alongside each other within one series is not quite the same as the likelihood of their appearance alone since a spike already present can influence the formation of another. Still, should the likelihood of forming an action potential be independent of the presence or timing of other spikes – that is, in case of statistically independent spikes – what we need is the firing rate to measure all likelihoods for probable action potential sequences.
In a simulation, using a firing rate-based model one will be able to simulate the temporal locations of those spikes by simulating an inhomogeneous Poisson process.

2.5.1 Point processes, Renewal processes and Poisson processes

A stochastic operation to form a series of events like action potentials in known as a point process. Commonly, the likelihood of such occurrences at random times may rely on the whole background of the previous events. In case such relation goes only as far as the single event before, thus making the intervals between successive ones independent, then the point process becomes a renewal process. On the other hand, should there be no such relation and dependence on previous events, thus making them statistically independent, then a Poisson process has taken place offering a highly efficient approximation of stochastic neuronal firing. For the sake of simplifying, we set apart the two - the homogeneous Poisson where the firing rate is steady through time, and the inhomogeneous Poisson where the firing rate must be time-dependent [40].

2.6 Poisson Processes

These find many applications in exceptional and arbitrary events in time or space. For instance radioactive radiation, road accidents, and action potentials [53].

2.6.1 Homogeneous Poisson Process

Take the underlying instantaneous firing rate r as constant over time – that is, a **homogeneous Poisson process**. Next, the inhomogeneous version is dealt with where $r(t)$ changes in time. With an extended interval $(0, T)$, we may position one spike within the interval and arbitrarily. Next, we choose a sub-interval (t_1, t_2) of length $\Delta t = t_2 - t_1$. As a consequence, the chance of a spike to appear during the sub-interval is $\Delta t/T$ [53].

At this point, we position k spikes in the $(0; T)$ interval and determine the likelihood that n of these spikes occur within the $(t_1; t_2)$ sub-interval. Here, the binomial formula asserts that:

$$P\{\text{spikes during } \Delta t\} = \frac{k!}{(k-n)!n!} p^n q^{k-n} \tag{2.1}$$

where: $p = \Delta t/T$ and $q = 1 - p$.
At this point, k and T are added and the ratio $r = k/T$ unchanged. Considering that k stands for the entire number of spikes and T for total time, $r = k/T$ represents the mean firing rate and the approximate number of spikes appearing each second. It may be proved that with $k \to \infty$, the likelihood of n spikes occurring in an interval of length Δt is as follows:

$$P\{\text{spikes during } \Delta t\} = e^{-r\Delta t} \frac{(r\Delta t)^n}{n!} \tag{2.2}$$

This expression is for the Poisson probability density function, considering the mean firing rate r, and the likelihood of n spikes appearing through a time interval of length Δt. This formulation works accurately only on the condition that the spikes occur

entirely separately and fall arbitrarily along an entire $(0, T)$ time interval. The number of spike in case of a homogeneous Poisson process can be determined as:

$$\langle n \rangle = \int_{t_1}^{t_2} r dt = r\Delta t \tag{2.3}$$

2.6.2 Inhomogeneous Poisson Process

The Poisson approach works in a similar way in case of time-varying firing rates, except that the constant r is replaced with a rate function $r(t)$ changing with time [53]. In case of an Inhomogeneous Poisson Process, the chance of detecting precisely n spikes in a given interval (t_1, t_2)) may be estimated as follows:

$$P\{\text{spikes during } (t_1, t_2)\} = e^{\langle n \rangle} \frac{(\langle n \rangle)^n}{n!} \tag{2.4}$$

CHAPTER 3

NEURON MODELLING, FITZHUGH NAGUMO EQUATIONS AND STOCHASTIC SIMULATION

3.1 Neuron Models

Otherwise regarded as the spiking neuron model, this is a numerical representation of certain nerve cell features creating major electrical potentials along the membrane in a time span of one millisecond. These models are applied in numerous attempts ranging from fundamental neural behavior studies to neuro-prosthetics.

Neuron simulation dates as far back as the middle of the 20th century, when the famous Hodgkin-Huxley (HH) framework was applied to quantitatively describe electrochemical processes in the squid giant axon [2]. Upon this major attempt, others like Morris- Lecar [3], Fitzhugh Nagumo [4] and Hindmarch - Rose [54] also followed – all of which supplied either additional information (like calcium channel dynamics) or reduced the general model to a fraction. Those attempting to simplify focus on a main process and do away with certain specifications and summarize all channels within one factor alone. To illustrate this, [3] explains the process of activation mechanism using a recovery factor and no other despite numerous such biophysical factors. Contrary to this approach, others like [4], [54] address behavioral specifications like repeated firing, bursting, and others – in this way excluding certain physical factors or merely including very few. In the light of the above information, in the present thesis we will examine a form of framework that explains the relationship between the input neuronal membrane current and output membrane voltage. Within this concept, the most comprehensive work was carried out by Hodgkin-Huxley – as stated earlier - in the early 50s with the help of an experimental arrangement making a hole in the cell

membrane to initiate a certain membrane voltage/current.

3.1.1 Hodgkin and Huxley model (HH)

The basic numerical model for present-day biophysical neural modeling was materialized almost half a century before by Alan Hodgkin and Andrew Huxley [2], who conducted a set of electro physiological tests on the squid giant axon.
This axon is famous for its unusual size of 0.5 *mm* since a majority of others in the squid nervous system and in general are commonly smaller by a minimum of 100 times. This dimension is characteristic and ideal for quick transmission of action potentials to initiate mantle contraction once the squid is running away from an aggressor. Apart from this advantage, this size helped Hodgkin and Huxley to make changes otherwise impossible in tiny axons for research purposes at the time. Through properly arranged tests, the two scientists revealed macroscopic ionic pulses in the squid giant axon being deciphered upon fluctuations in Na^+ and K^+ conductance within the membrane. Within a set of voltage-clamp tests, they formed an intricate numerical framework for the voltage-reliant as well as time-reliant characteristics of the Na^+ and K^+ conductance. These experiments paved the way for a dual series of differential formulas for the ionic basis of the action potential (Hodgkin and Huxley, 1952) – later labeled the Hodgkin-Huxley (HH) model. The actual predictability of this framework was made clear once they showed that the application of their formulas – applying a manually operated mechanical calculator – correctly generated all the major biophysical features of the action potential. Against their success, Hodgkin and Huxley received the Nobel Prize in Physiology and Medicine in 1963. The primary equation is a fourth-order nonlinear model as appears below:

$$\begin{aligned} C_m \frac{\mathrm{d}V_m}{\mathrm{d}t} &= -\bar{g}_{\mathrm{K}} n^4 (V_m - V_K) - \bar{g}_{\mathrm{Na}} m^3 h (V_m - V_{Na}) - \bar{g}_l (V_m - V_l) + I_{ext} \\ \frac{dn}{dt} &= \alpha_n(V_m)(1-n) - \beta_n(V_m) n \\ \frac{dm}{dt} &= \alpha_m(V_m)(1-m) - \beta_m(V_m) m \\ \frac{dh}{dt} &= \alpha_h(V_m)(1-h) - \beta_h(V_m) h \end{aligned} \tag{3.1}$$

where V_m is the membrane potential in mV, n, m, h are dimensionless variables that stands for the potassium (K^+) channel activation, sodium (Na^+) channel activation and inactivation respectively. In other words they are the relative concentration of respective ions. They are in the interval [0, 1]. The $\alpha_n(V_m)$, $\beta_n(V_m)$, $\alpha_m(V_m)$, $\beta_m(V_m)$,$\alpha_h(V_m)$ and $\beta_h(V_m)$ are functions of membrane potential as shown below:

$$\begin{aligned} \alpha_n(V_m) &= \frac{0.01(V_m+10)}{\exp\left(\frac{V_m+10}{10}\right)-1} \qquad \alpha_m(V_m) = \frac{0.1(V_m+25)}{\exp\left(\frac{V_m+25}{10}\right)-1} \qquad \alpha_h(V_m) = 0.07\exp\left(\frac{V_m}{20}\right) \\ \beta_n(V_m) &= 0.125\exp\left(\frac{V_m}{80}\right) \quad \beta_m(V_m) = 4\exp\left(\frac{V_m}{18}\right) \qquad \beta_h(V_m) = \frac{1}{\exp\left(\frac{V_m+30}{10}\right)+1} \end{aligned} \tag{3.2}$$

The definitions and nominal values of the parameters are: $g_K = 36$ mS/cm^2 the conductance of the potassium channel, $g_Na = 120$ mS/cm^2 the conductance of the sodium channel, $g_l = 0.3$ mS/cm^2 the conductance of the channel representing leakage, $V_K = 36$ mV the equilibrium potential of the potassium channel, $V_{Na} = 115$ mV the equilibrium potential of the sodium channel and $V_l = 36$ mV the equilibrium potential of the channel representing leakage. In (3.1), I represents the current injected in mA/cm^2 from external sources (i.e. either a surrounding neuron or manual injection). When $I = 0$, one can see the response of the HH neuron with the nominal parameters in **Figure 3.1**.

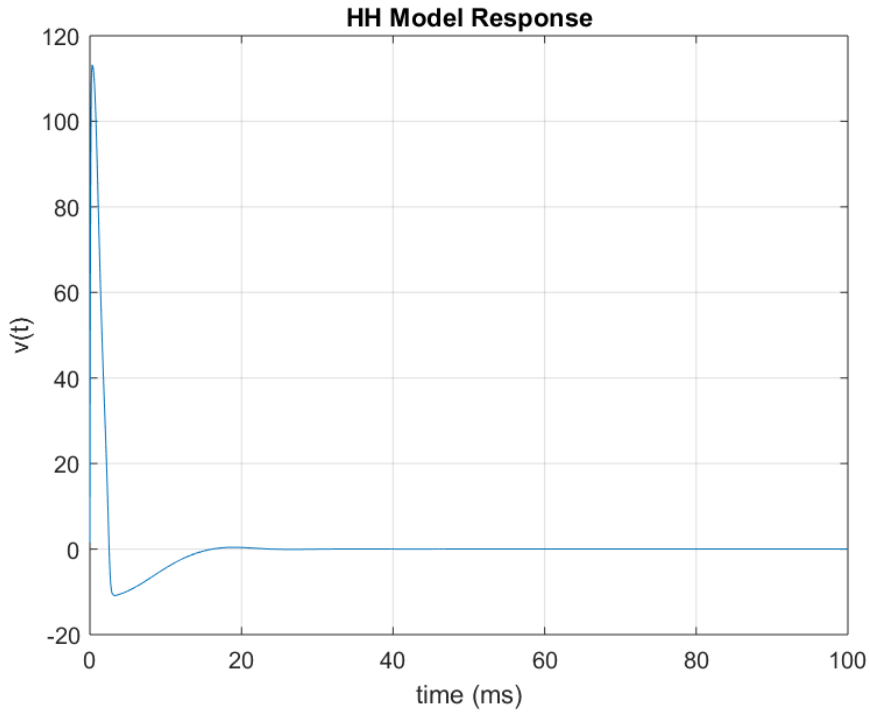

Figure 3.1: The response of HH model with the nominal values of parameters

Accordingly, the response appears as roughly an actual single action potential.

3.1.2 FitzHugh-Nagumo model (FHN)

The FHN framework is a separate attempt formed by Fitzhugh [55] and Nagumo [56] and away from the HH model. Based on formulas (3.1) and (3.2), one can argue that because the time scales for m, n, and h did not belong to one order, many hypotheses could be formed as a result; such that m may be made redundant as it is the opening of the sodium gates in the membrane. In relative terms, this incident occurs instantly and, as such, $dm\ dt = 0$. As the system continues to preserve a majority of the factors seen throughout the test, once h is assigned as equal to a constant h_0, it (h) may as well be disregarded. The HH model, in this way, became simplified within a rather more identifiable framework, yielding a 2-component (V, W) model defined within a dimension-free set as:

$$\begin{aligned} \dot{V} &= V - dV^3 - W + I \\ \dot{W} &= cV + a - bW \end{aligned} \tag{3.3}$$

Here, (a, b, c, d) represent certain neuron parameters, (V) appears in mV's, and (I) in $\mu A/cm^2$. Furthermore, this formula suggests that time factor t is in milliseconds. **Table 3.2** depicts the nominal figures related to the specific parameters of (3.9). The framework to form action potential in neurons – regarded as the Fitzhugh Nagumo (FN) model and dissimilar to the HH framework of 4 dynamical variables – merely comprises 2 variables and, in this way, can examine all the potentials thanks to phase plane techniques.

The Fitzhugh-Nagumo (FHN) framework, in a sense, summarizes the HH approach to examine the potential action of giant squid axons.

Table 3.1: The nominal parameters of the FN model in (3.9)

Parameter	Value
a	0.08
b	0.056
c	0.064
d	0.333

It can be seen that all changes in membrane potential values as per the parameters in **Table 3.2** are identical to those in **Figure 3.2**.

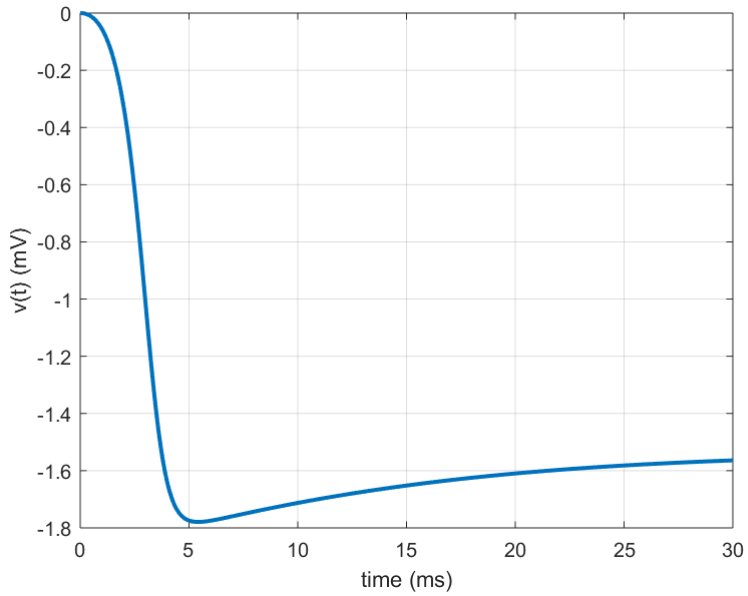

Figure 3.2: Variation of the membrane potential

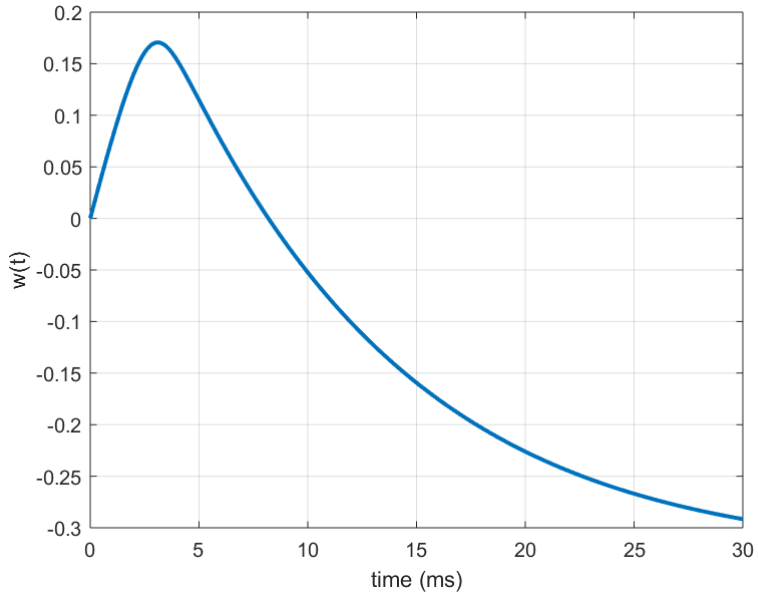

Figure 3.3: Variation of the recovery variable

To make reference between the membrane potential and the neural firing rate, we require a nonlinear map like that of a logistic sigmoid function, as appears in the following [57]:

$$r(t) = \frac{F}{1 + \exp(-v(t))} \tag{3.4}$$

Here, F represents the maximum firing rate, and $F = 100$ offers a firing response as exemplified in 3.4.

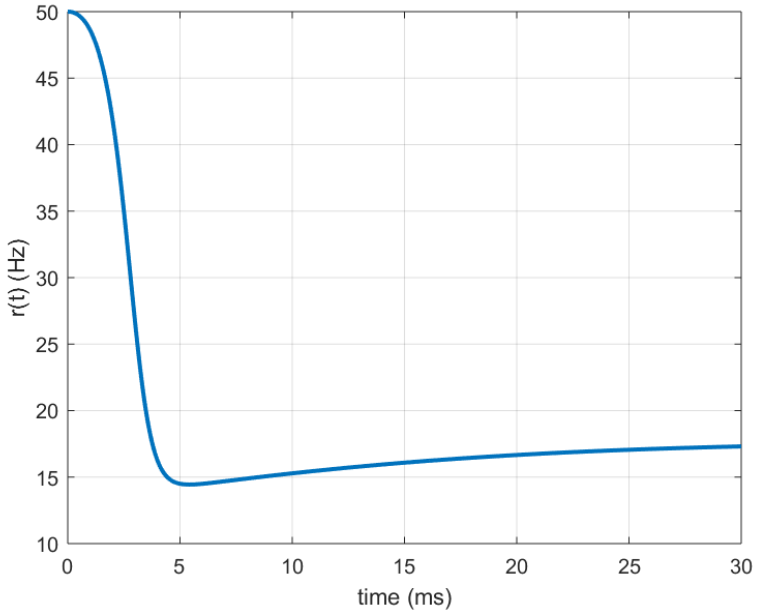

Figure 3.4: FitzHugh-Nagumo neural firing rate variation.

As commonly carried out, the neural information appears in code within the distribution of the tips of the repeated action potentials, regarded as spikes. Furthermore, in actual in-vivo settings, such spiking occurs dependent on the firing rate $r(t)$. Other studies have revealed that such spikes follow an inhomogeneous inconsistent Poisson pattern [58, 59] explained as:

$$\text{Prob}\left[N(t + \Delta t) - N(t) = k\right] = \frac{e^{-\lambda}\lambda^k}{k!} \tag{3.5}$$

where

$$\lambda = \int_t^{t+\Delta t} r_e(\tau)\, d\tau \tag{3.6}$$

represent the mean number of spikes according to the firing rate$r_e(t)$ and dependent on time; whereas $N(\tau)$ shows the entire number of spike events until the time τ, in a

way that $N(t+\Delta t) - N(t)$ stands for spikes in time interval $[t, t+\Delta t)$.
Put in different terms, the chance of experiencing k number of spikes in the interval $(t, t+\Delta t)$ can be measured as per the Poisson distribution mentioned earlier.
Take a spike train $(t_1, t_2, \ldots, t_K)$ in the time interval $(0, T)$ (here $0 \leq t_1 \leq t_2 \leq \ldots \leq t_K \leq T$ so t and Δt become $t = 0$ and $\Delta t = T$). Here the spike train is described by a list of the time stamps for the K spikes. At this point, the train can be defined using a series of time stamps for K spikes.
The probability density function for a hypothetical spiking train $(t_1, t_2, \ldots, t_K)$ may, then, be obtained based on the Poisson pattern [60, 61], yielding:

is the mean number of spikes based on the firing rate $r_e(t)$ which varies with time, and $N(\tau)$ indicates the cumulative total number of spikes up to time τ, so that $N(t+\Delta t) - N(t)$ is the number of spikes within the time interval $[t, t+\Delta t)$.

In other words, the probability of having k number of spikes in the interval $(t, t+\Delta t)$ is given by the Poisson distribution above.

Consider a spike train $(t_1, t_2, \ldots, t_K)$ in the time interval $(0, T)$ (here $0 \leq t_1 \leq t_2 \leq \ldots \leq t_K \leq T$ so t and Δt become $t = 0$ and $\Delta t = T$). Here the spike train is described by a list of the time stamps for the K spikes. The probability density function for a given spiking train $(t_1, t_2, \ldots, t_K)$ can be derived from the inhomogeneous Poisson process [43, 61]. The result reads:

$$p(t_1, t_2, \ldots, t_K) = \exp\left(-\int_0^T r_e(t, \mathbf{x}, \theta)\, dt\right) \prod_{k=1}^{K} r_e(t_k, \mathbf{x}, \theta) \tag{3.7}$$

Such a probability density explains the chance of a given spike train $(t_1, t_2, \ldots, t_K)$ being formed due to the Poisson pattern at the rate function $r_e(t, \mathbf{x}, \theta)$., Obviously, such a rate function relies entirely upon the network factors as well as the applied stimulus. Here, the functions are employed as possibilities.
For the purpose of illustrating a Poisson event, we may apply the local Bernoulli approximation [10] appearing in brief as follows: This probability density describes how likely a particular spike train $(t_1, t_2, \ldots, t_K)$ is generated by the inhomogeneous Poisson process with the rate function $r_e(t, \mathbf{x}, \theta)$., Of course, this rate function depends implicitly on the network parameters and the stimulus used. We will use these functions as likelihoods.

To simulate a Poisson process one can use the local Bernoulli approximation [43]. The procedure can be summarized as follows:

1. Assuming a firing rate of a given neuron as $r(t)$.
2. Determine the likelihood of firing at time t_i through $p_i = r(t_i)\Delta t$ where Δt represents integration interval brief as 1ms.
3. Calculate a given variable upon taking an example of a distribution uniform between 0 and 1, defined as Define this as $x_{rand} = U[0, 1]$ where U stands for uniform distribution.
4. If $p_i > x_{rand}$ releases a spike at $t = t_i$, else do nothing.
5. Gather all spikes as $S = [t_1, \ldots, t_{N_s}]$ where N_s represents the number of spikes collected in one round of simulation.

Carrying out this process using a bin size of $\Delta t = 0.001$, we can collect a neural spiking profile like the one in Figure 3.5, not to forget that since the time base of the FN model counts in milliseconds $\Delta t = 0.001$ equals a bin size of 1 μs.

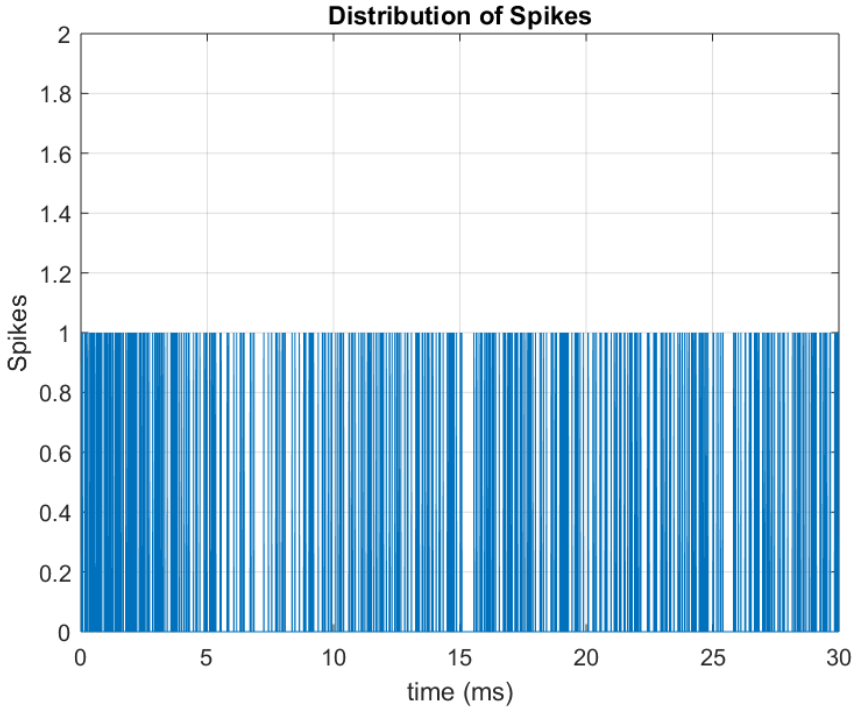

Figure 3.5: Simulation of neural spiking corresponding to the firing rate profile in Figure 3.4

3.2 Modeling of the Stimulus

So far in the study, all simulations have been carried out in the absence of external stimulus. Generally speaking, neurons react to any given stimulation, namely light, sound, motion, or else. In our work, we apply an electric current arranged in advance. In the auditory cortex region of the brain, there exists a tono-topically arranged axis in the sound processing subsystem beginning from the basilar membrane of the ear toward the auditory cortex located at the mid-brain. In this way, one may consider a series of reactive to a limited scope frequencies. Once the input to the neuron (as the FN system employed in this study) originates from a tonotopically arranged series of neurons, we may create a stimulus to the neuron in the form of a Fourier Series pulse and simulate using a phased cosine Fourier setting in the following way [33]

$$I = \sum_{n=1}^{N_U} A_n \cos\left(\omega_n t + \phi_n\right) \tag{3.8}$$

Here, A_n represents the amplitude, $\omega_n = 2\pi f_0 n$ stands for the frequency of the n-th Fourier component in radians/sec, and finally ϕ_n shows the phase of the component. Amplitude A_n and base frequency f_0 (in Hz) remain unchanged, whereas phase ϕ_n shall be a random one picked from a uniform distribution between the $[-\pi,\ \pi]$ radians. The amplitude parameter A_n is constant in all modes of n as $A_n = A_{\max}$.

If $A_{\max} = 20$, $\omega_n = 3n$, $N_U = 5$ and the phase randomly chosen can generate a stimulus in the same way as in Figure 3.6, and the respective membrane potential and the firing rate responses as in Figures 3.7 and 3.8, respectively. As for the anticipated neural spiking profile, Figure 3.9 clearly shows it.

3.3 FitzHugh-Nagumo Equations Delivering the Firing Rate

Fitzhugh–Nagumo (FHN) model is a second-order polynomial nonlinear differential equation bearing two states representing the membrane potential (V) and a recovery variable (W), which lumps all ion channel related processes into one state. Mathematically, it can be represented as shown below [62]:

$$\begin{aligned} \dot{V} &= V - dV^3 - W + I \\ \dot{W} &= cV + a - bW \end{aligned} \tag{3.9}$$

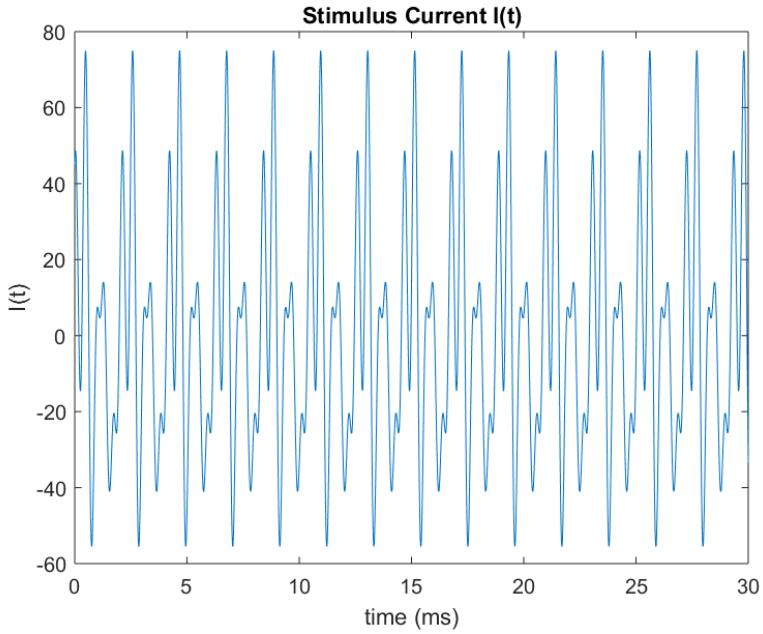

Figure 3.6: A Fourier Series stimulus for $A_{\max} = 20$, $\omega_n = 3n$, $N_U = 5$ and phase randomly assigned

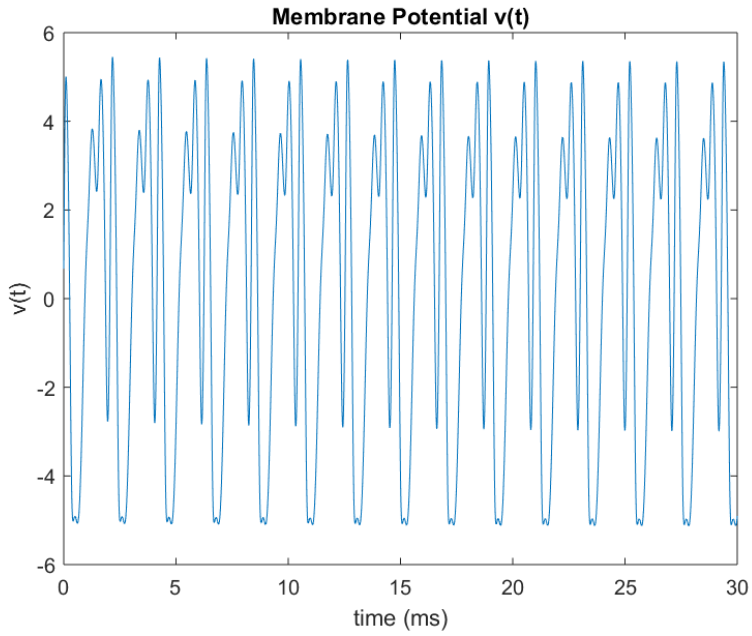

Figure 3.7: Membrane potential response of Fitzhugh-Nagumo neuron to the stimulus in Figure 3.6

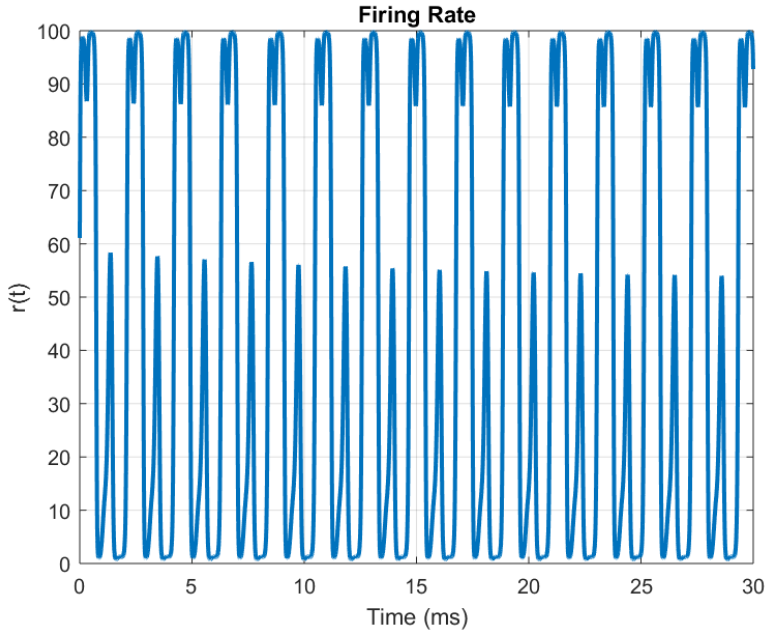

Figure 3.8: Membrane potential response of Fitzhugh-Nagumo neuron to the stimulus in Figure 3.6

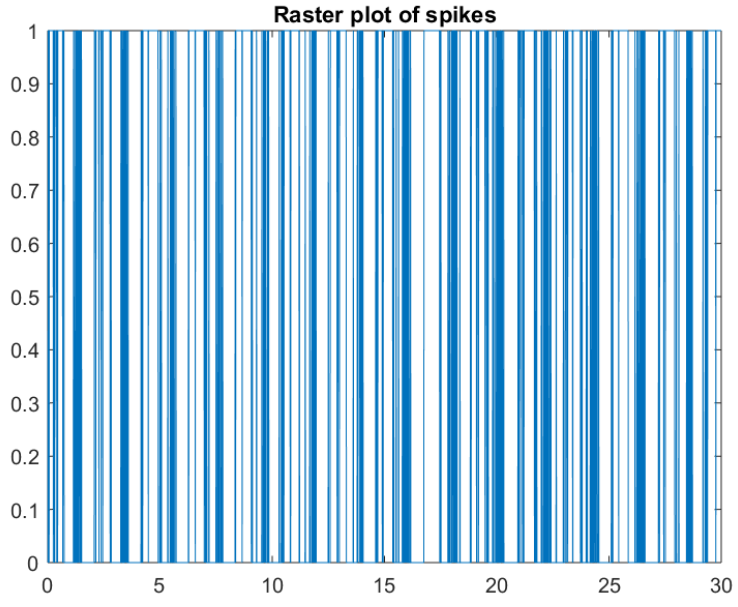

Figure 3.9: Firing rate response of Fitzhugh-Nagumo neuron to the stimulus in Figure 3.6

The above model has four parameters $[a, b, c, d]$ determining its properties. In the original text associated with the FN models, the coefficient of the V^3 is $1/3$; however, in this work, we suppose that the coefficient of that cubic term is not constant and we assign a parameter d to it. In Equation (3.9), I represents the stimulus exciting the neuron. It can be thought of as an electric current.

In the introduction, we state that we need a relationship between the membrane potential representative variable V and the firing rate of our neuron. In addition, we also state that we can construct such a map by developing a nonlinear sigmoidal map as shown below:

$$r = \frac{F}{1 + \exp(-V))} \tag{3.10}$$

where r is the firing rate of the neuron in ms^{-1} and F is the maximum firing rate parameter. Thus, one has five parameters to estimate and they can be vectorally expressed as:

$$\theta = [a, b, c, d, F] \tag{3.11}$$

Thus, we can call $\hat{\theta}$ as the estimates of θ. In the application, we needed the true values of θ so that we coul generate the spikes that represent the collected data from a realistic experiment. These are available in Table 3.2.

Table 3.2: The nominal parameters of the FN model in Equations (3.9) and (3.10). These were evaluated using the information in [1].

Parameter	**Value**
a	0.08
b	0.056
c	0.064
d	0.333
F	100

3.4 Neural Spiking and Point Processes

We state in the introduction that the neural spiking is a point process that largely obeys an Inhomogeneous Poisson Process (IPP). A basic Poisson process is characterized by

an event rate λ and has an exponential probability mass function defined by:

$$\text{Prob}\left[N\left(t+\Delta t\right)-N\left(t\right)=k\right]=\frac{e^{-\lambda}\lambda^{k}}{k!} \tag{3.12}$$

where k is the number of events that occur in the interval $[t, t+\Delta t)$. In the simplest case, λ is constant in that interval. In neural operation, the process is much more complex and assuming a constant event rate is insufficient; thus, we refer to a time varying event rate, which is actually equivalent to the firing rate $r(t)$ of the neuron (refer to Equation (3.10)). This yields an inhomogeneous Poisson point process with the event rate λ replaced by the mean firing rate defined by:

$$\lambda=\int_{t}^{t+\Delta t} r\left(\tau\right)d\tau \tag{3.13}$$

Now, the term k represents the spike count in the interval $[t, t+\Delta t)$, which is statistically related to the firing rate $r(t)$; λ now represents the mean spike count for the firing rate $r(t)$, which varies with time; and $N(\tau)$ stands for the cumulative total number of spikes up to time τ, thus making $N\left(t+\Delta t\right)-N\left(t\right)$ the spike count for the time interval $[t, t+\Delta t)$.

Now, let us take a spike train $(t_1, t_2, \ldots, t_K)$ in the time interval $(0, T)$. Here, $0 \leq t_1 \leq t_2 \leq \ldots \leq t_K \leq T$, thus t and Δt become 0 and T. The spike train can be defined using a series of time stamps for K spikes. As a result, the likelihood density function related to any spike train $(t_1, t_2, \ldots, t_K)$ is gained using an inhomogeneous Poisson process [63, 61] in the following way:

$$p\left(t_1, t_2, \ldots, t_K\right)=\exp\left(-\int_{0}^{T} r\left(t, \mathbf{x}, \theta\right)dt\right)\prod_{k=1}^{K} r\left(t_k, \mathbf{x}, \theta\right) \tag{3.14}$$

The function reveals the likelihood of a given spike train $(t_1, t_2, \ldots, t_K)$ to occur with the rate function $r\left(t, \mathbf{x}, \theta\right)$, which obviously is relying mainly upon network parameters and the stimulus applied.

$$p\left(t_1, t_2, \ldots, t_K\right)=\exp\left(-\int_{0}^{T} r\left(t, \mathbf{x}, \theta\right)dt\right)\prod_{k=1}^{K} r\left(t_k, \mathbf{x}, \theta\right) \tag{3.15}$$

The function reveals the likelihood of a given spike train $(t_1, t_2, \ldots, t_K)$ to occur with

the rate function $r(t, \mathbf{x}, \theta)$, which obviously is relying mainly upon network parameters and the stimulus applied.

3.5 Maximum Likelihood Methods and Parameter Estimation

The parameters requiring assessment appear as a vector:

$$\theta = [\theta_1, \ldots, \theta_5] = \left[\hat{\theta}_1, \ldots, \hat{\theta}_5\right] \tag{3.16}$$

to cover all the parameters in Equation (3.11). The maximum probability here relies on the function proposed in Equation (3.15) and includes each spike timing as well. Estimation theory asserts that determining maximum probability is asymptotically effective and goes as far as the Cramér–Rao bound within the scope of large data. Therefore, for us to expand the probability function in Equation (3.15) to further cover settings with numerous spike trains initiated by numerous stimuli, a series of M stimuli should be assumed. Take the mth stimulus ($m = 1, \ldots, M$) to initiate a spike train containing K_m spikes in the time window $[0, T]$, and the spike timings are given by $S_m = \left(t_1^{(m)}, t_2^{(m)}, \ldots, t_{K_m}^{(m)}\right)$. By Equation (3.15). According to Equation (3.15), the probability function for the spike train S_m can be determined as:

$$p(S_m \mid \theta) = \exp\left(-\int_0^T r^{(m)}(t)\, dt\right) \prod_{k=1}^{K_m} r^{(m)}\left(t_k^{(m)}\right) \tag{3.17}$$

in which $r^{(m)}$ represents the firing rate due to the mth stimulus. Let us denote that the rate function $r^{(m)}$ entirely relies on the parameters related to neuron parameters θ and the stimulus. On the left-hand side of Equation (3.17), its reliance on the neuron parameters θ can be noted.

Supposing the stimulus and its elicited responses in each mth trial are independent, one can derive a joint likelihood function as:

$$L(S_1, S_2, \ldots, S_M \mid \theta) = \prod_{m=1}^{M} p(S_m \mid \theta) \tag{3.18}$$

To improve its convexity, we can make use of natural logarithm and derive a log likelihood function as shown below:

$$l(S_1, S_2, \ldots, S_M \mid \theta) = -\sum_{m=1}^{M} \int_0^T r^{(m)}(t)\, dt + \sum_{m=1}^{M} \sum_{k=1}^{K_m} \ln r^{(m)}\left(t_k^{(m)}\right) \tag{3.19}$$

Finally, the maximum likelihood estimates of the parameter vector θ is obtained by:

$$\hat{\theta}_{ML} = \arg\max_{\theta} [l(S_1, S_2, \ldots, S_M \mid \theta)] \tag{3.20}$$

3.6 Spike Generation for Data Collection

Since this study was of computational type and targeted the development of an algorithm to be applied in a realistic experiment, we needed a solid approach to generate a dataset to represent the output of a realistic experiment. In the current research, the data were a set of neural spike trains that bear the individual spike timings with no amplitude information. In addition, we also know that the neural spiking process largely obeys inhomogeneous Poisson statistics, thus we could achieve that goal by implementing a stable Poisson process simulation. In other words, we simulated an inhomogeneous Poisson process with $r(t)$ as its event rate. There are several algorithms to simulate an inhomogeneous Poisson process. The local Bernoulli approximation [60], thinning [64], and time scale transformation [65] can be shown as examples.

If the time bin is sufficiently small such that only one spike is fitted, one can use local Bernoulli approximation to generate the neural spiking data very easily. The is also a reasonable choice when the neuron models are integrated by discrete solvers such as the Euler or Runge–Kutta method. One can see a summary of the related algorithm below [33]:

1. Given the firing rate of a neuron as $r(t)$.
2. Find the probability of firing at time t_i by evaluating $p_i = r(t_i)\delta t$ where δt is the integration interval. It should be a small real number such as 1 ms.
3. Draw a random number $x_{rand} = U[0, 1]$ that is uniformly distributed in the interval $[0, 1]$. Here, U stands for a uniform distribution.
4. If $p_i > x_{rand}$, fire a spike at $t = t_i$, else do nothing.
5. Collect spikes as $S = [t_1, \ldots, t_{N_s}]$ where N_s will be the total number of spikes collected from one simulation.

CHAPTER 4

APPLICATION

In this section, we introduce a simulation-based approach to evaluate the parameters of a firing rate-based single Fitzhugh–Nagumo neuron model. The process in brief appears as follows:

1. A single run of simulation lasted for $T_f = 30$ ms.
2. The stimulus amplitude $A_{\max}$ and base frequency f_0 were assigned prior to each trial m. The phase angles ϕ_n was assigned randomly, as defined in Section **??**.
3. The firing rate profile was obtained by integrating the FN model in Equation (3.9) for $T_f = 30$ ms using a time bin of The integration was performed at the true values of the parameters in Table 3.2 to generate the actual firing rate information $r^m(t)$ of current mth trial.
4. Using the approach presented in Section 3.6, the spike train S_m of the mth trial was generated from the firing rate $r^m(t)$. The number of spikes was K_m at the mth trial.
5. The simulation was repeated N_{it} times to collect several statistically independent spike trains, i.e., $m = 1 \ldots N_{it}$.
6. The neural spiking data needed by Equation (3.19) were obtained at the fifth step. However, the firing rate $r^m(t)$ in Equation (3.19) should be computed at the current iteration of the optimization.
7. An optimization algorithm (e.g., `fmincon`) was run on the joint likelihood function in Equation (3.19) to obtain the maximum likelihood estimates of the pa-

rameters (θ_{ML} in Equation (3.20)).

4.1 Optimization Algorithm

To perform a maximum likelihood estimation (i.e., the problem defined in Equation (3.20)), we needed an optimizer. Most optimizers target a local minimum and thus require multiple initial guesses to increase the probability of finding a global optimum to the problem. However, this is a time consuming task and in a problem similar to that of this research duration is a crucial parameter. This was even more critical when we are using our algorithms in a physiological experiment. Some optimization algorithms such as genetic, pattern search, or simulated annealing do not require the online computation of gradients but they are computationally extensive and will most likely require a longer duration. Thus, in this research, we preferred a gradient based algorithm and utilized MATLAB's `fmincon` routine. It is based on interior-point algorithms (a modified Newton's method) and allows lower and upper bounds to be set on the result. As all parameters of an FN model are positive, a zero lower bound will prevent unnecessary parameter sweeps.

4.2 Simulation Scenarios

In this section, we introduce the results related to parameter estimation using table for the variation of mean estimated values $\hat{\theta} = \left[\hat{\theta}_1, \hat{\theta}_2, \hat{\theta}_3, \hat{\theta}_4, \hat{\theta}_5\right]$ of parameters $\theta = [\theta_1, \theta_2, \theta_3, \theta_4, \theta_5] = [a, b, c, d, F]$. The scenario information for the present problem appear in Table 4.1. To show impact of various stimulus components N_U, amplitude level $A_{\max}$, and number of trials N_{it}, the problem was re-run for a set of different values of those parameters. The initial conditions of the states representing the membrane potential V and recovery activity W in Equation (3.9) were assumed as $V(0) = 0$ and $W(0) = 0$. This is a reasonable choice as we did not have any information about them. **A typical stimulus response relationship can be seen in Figure 4.1. Here, the stimulus parameters are $A_{\max} = 100$, $f_0 = 10/3$ kHz, and $N_U = 5$. The nominal parameters in Table 3.2 were used in this simulation.**

Table 4.1: Data for the simulation scenario.

Parameter	**Symbol**	**Value**
Simulation Time	T_f	30 ms.
Number of Trials	N_{it}	25, 50, 100, 200
# of Components in Stimulus	N_U	5, 10, 20, 30
Method of Optimization	N/A	Interior-Point Gradient Descent (MATLAB)
# of True Parameters	Size(θ)	5
Stimulus Amplitude (μA)	$A_{\max}$	25, 50, 100, 200
Base Frequency	f_0	$\frac{1}{3}$, 1, $\frac{7}{3}$, $\frac{10}{3}$ KHz

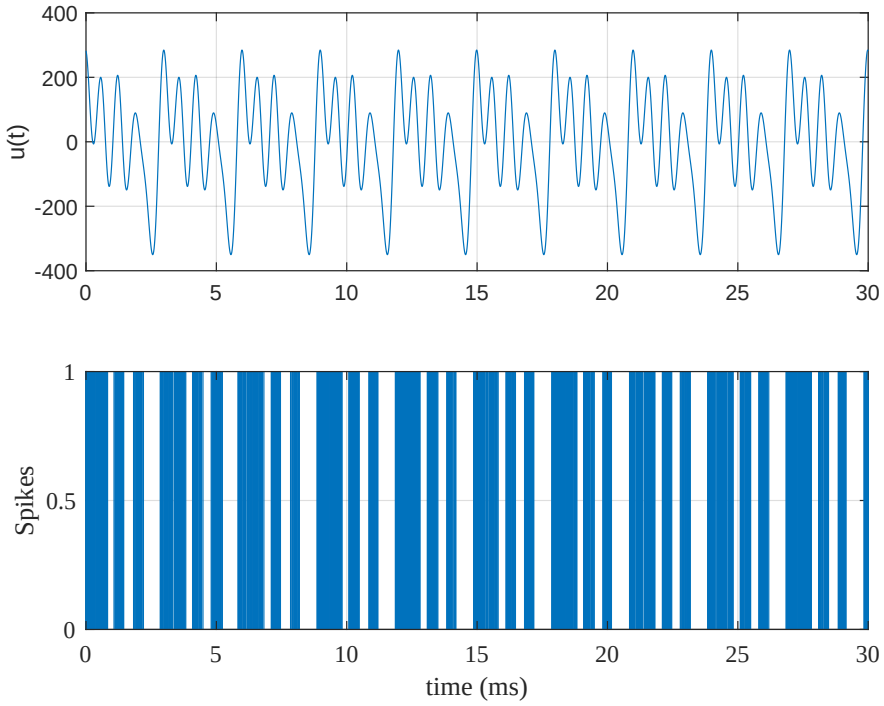

Figure 4.1: A typical stimulus and response pattern. In the first pane, a Fourier series stimulus with parameters $A_{\max} = 100$, $f_0 = 333$ Hz, and $N_U = 5$ is displayed. In the second pane, the neural spiking pattern of the Fitzhugh–Nagumo model in Equation (3.9) with the nominal parameters in Table 3.2 obtained after Poisson simulation can be seen.

4.2.1 Estimation of Parameters Using a Realistic Data

As stated in the end of the Introduction, we were likely interested in the results of the estimation when the stimulus/response data (spike trains collected) were collected from realistic neurons. Although performing an experiment may not be possible, one can use data from repositories or other sites on the web. We used the data collected in an experiment performed by [66]. Here, the stimulus was of white noise type and the response was measured from H1 neurons of blowfly vision system. The data are available as a MATLAB workspace file on the website In this dataset, a single stimulus of 20 min duration stimulates the H1 neurons of the flies. We divided these 1200 s long data into 2400 segments, each of which is 500 ms long. Thus, our algorithm was applied as if there were 2400 independent stimuli of 500 ms duration. Since we had a random stimulus here, we could assume that segments were triggered by independent stimuli. The algorithm was provided by subsets of data having 25, 50, 100, 200, 300, 400, 500, 600, 700, 800, 900, 1000, 1100, 1200, 1300, 1400, 1500, 1600, 1700, 1800, 1900, 2000, 2100, 2200, 2300, and 2400 samples (in other words, the value of N_{it}).

CHAPTER 5

RESULTS

5.1 Results

In this chapter, the results of our example problem are presented. The maximum likelihood estimates (θ_{ML}) of the parameters (θ) in Equation (3.11) were obtained by maximizing Equation (3.18) using MATLAB's `fmincon` routine. The relevant results can be categorized under two headings :

1. The variations of mean estimated values of θ (θ_{ML}) against varying sample size N_{it}, amplitude level $A_{\max}$, stimulus component size N_U, and base frequency f_0 are presented in Section 5.1.1.

2. The variations of standard deviations of the estimated parameters against varying sample size N_{it}, amplitude level $A_{\max}$, stimulus component size N_U, and base frequency f_0 are presented in Section 5.1.2.

5.1.1 Mean Estimated Values

One can see the variation of the mean estimated values of each parameter in Equation (3.11) against the number of samples N_{it}, amplitude $A_{\max}$, component size N_U, and base frequency f_0 of the stimulus in Tables 5.1–5.4, respectively.

Table 5.1: Estimated value vs. N_{it} ($N_U = 5$, $A_{max} = 100$, and $f_0 = 333.3$ Hz).

N_{it}	$\hat{\theta}_1$	$\hat{\theta}_2$	$\hat{\theta}_3$	$\hat{\theta}_4$	$\hat{\theta}_5$
5	0.0781	0.0504	0.0627	0.3348	100.0135
50	0.0953	0.0816	0.0731	0.3317	99.9960
100	0.0870	0.0635	0.0695	0.3326	99.9933
200	0.0840	0.0597	0.0694	0.3325	100.0065

Table 5.2: Estimated value vs. N_U ($N_{it} = 100$, $A_{max} = 100$, and $f_0 = 333.3$ Hz).

N_U	$\hat{\theta}_1$	$\hat{\theta}_2$	$\hat{\theta}_3$	$\hat{\theta}_4$	$\hat{\theta}_5$
5	0.0781	0.0504	0.0627	0.3348	100.0135
10	0.0811	0.0436	0.0595	0.3333	99.9927
20	0.0849	0.0618	0.0801	0.3326	99.9943
30	0.0770	0.0505	0.0636	0.3331	99.9920

Table 5.3: Estimated value vs. $A_{\max}$ ($N_{it} = 100$, $N_U = 5$, and $f_0 = 333.3$ Hz).

A_{max}	$\hat{\theta}_1$	$\hat{\theta}_2$	$\hat{\theta}_3$	$\hat{\theta}_4$	$\hat{\theta}_5$
25	0.0817	0.0549	0.0638	0.3337	99.9980
50	0.0809	0.0586	0.0699	0.3330	100.0008
100	0.0781	0.0504	0.0627	0.3348	100.0135
200	0.0767	0.0505	0.0608	0.3322	99.9894

Table 5.4: Estimated value vs. f_0 ($N_{it} = 100$, $N_U = 5$, and $A_{max} = 100$). Frequencies are in KHz.

f_0	$\hat{\theta}_1$	$\hat{\theta}_2$	$\hat{\theta}_3$	$\hat{\theta}_4$	$\hat{\theta}_5$
1/3	0.0856	0.0637	0.0712	0.3315	99.9942
1	0.0796	0.0550	0.0641	0.3364	100.0124
5/3	0.0861	0.0566	0.0627	0.3327	100.0195
7/3	0.0870	0.0635	0.0695	0.3326	99.9933

5.1.2 Standard Deviations

One can see the variation of the standard deviations of the estimates of each parameter in Equation (3.11) against the number of samples N_{it}, amplitude $A_{\max}$, component size N_U, and base frequency f_0 of the stimulus in Tables 5.5–5.8, respectively.

Table 5.5: Standard deviations vs. N_{it} ($N_U = 5$, $A_{max} = 100$, and $f_0 = 333.3$ Hz).

N_{it}	$\sigma(\theta_1)$	$\sigma(\theta_2)$	$\sigma(\theta_3)$	$\sigma(\theta_4)$	$\sigma(\theta_5)$
5	0.0423	0.0487	0.0366	0.0057	0.0895
50	0.0350	0.0387	0.0321	0.0021	0.0770
100	0.0339	0.0446	0.0246	0.0017	0.0634
200	.0235	0.0343	0.0276	0.0023	0.02995

Table 5.6: Standard deviations vs. N_U ($N_it = 100$, $A_{max} = 100$, and $f_0 = 333.3$ Hz).

N_U	$\sigma(\theta_1)$	$\sigma(\theta_2)$	$\sigma(\theta_3)$	$\sigma(\theta_4)$	$\sigma(\theta_5)$
5	0.0258	0.0345	0.0196	0.0024	0.0399
10	0.0287	0.0406	0.0356	0.0016	0.0444
20	0.0337	0.0457	0.0485	0.0015	0.0499
30	0.0165	0.0204	0.0149	0.0016	0.0189

Table 5.7: Standard deviations vs. A_{max} ($N_it = 100$, $N_U = 5$, and $f_0 = 333.3$ Hz).

A_{max}	$\sigma(\theta_1)$	$\sigma(\theta_2)$	$\sigma(\theta_3)$	$\sigma(\theta_4)$	$\sigma(\theta_5)$
25	0.0151	0.0216	0.0137	0.0022	0.0671
50	0.0181	0.0275	0.0232	0.0023	0.0640
100	0.0258	0.0345	0.0196	0.0024	0.0399
200	0.0311	0.0388	0.0289	0.0034	0.0264

Table 5.8: Standard deviations vs. f_0 ($N_it = 100$, $N_U = 5$, and $A_{max} = 100$). The frequencies are in KHz.

f_0	$\sigma(\theta_1)$	$\sigma(\theta_2)$	$\sigma(\theta_3)$	$\sigma(\theta_4)$	$\sigma(\theta_5)$
1/3	0.0178	0.0312	0.0158	0.0043	0.0407
1	0.0129	0.0165	0.0067	0.0064	0.0329
5/3	0.0258	0.0364	0.0254	0.0034	0.0447
7/3	0.0339	0.0446	0.0246	0.0017	0.0634

In addition to the tabular results, the variation of the standard deviations are also presented in graphical forms in Figures 5.1–5.4.

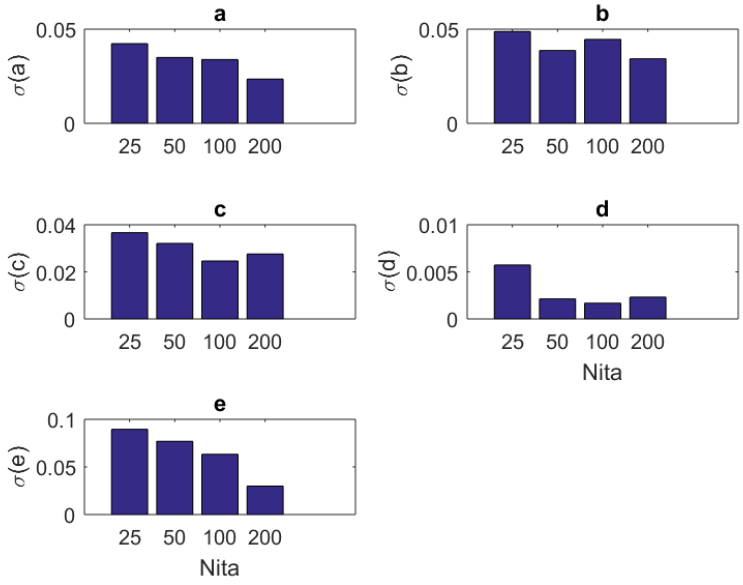

Figure 5.1: The variation of individual (relative errors SD) of the estimates against varying sample (iteration) size N_{it}. Where $N_U = 5$, $A_{\max} = 100$, and $f_0 = 333.3$ Hz. For most parameters, these relative errors show an improving behavior with the increasing sample size. However, some parameters such as b do not present any improvement or degradation in relative errors. However, in general, the relative error levels remain small.

5.1.3 Results of Estimation from Realistic Data

As mentioned in Section 4.2.1, we also utilized realistic data obtained from H1 neurons of blowflies [66]. A little more detailed discussion is available in Section 4.2.1. The variation of estimated values of neuron parameters a, b, c, d, F against the sample sizes are available in Table 5.9. In Table 5.10, the relative error with respect to the case with previous sample size setting is shown. The relative error was computed with the following scheme:

$$ER(k) = \frac{\left(\hat{\theta}(k) - \hat{\theta}(k-1)\right)}{\hat{\theta}(k-1)} \tag{5.1}$$

where k refers to each of the cases in Table 5.9 and they are identified by the sample size parameter N_{it}. Here, k did not start from $k = 1$ because we did not have any data concerning the cases $N_{it} < 25$. Thus, in Table 5.10, the k value starts from $k = 2$.

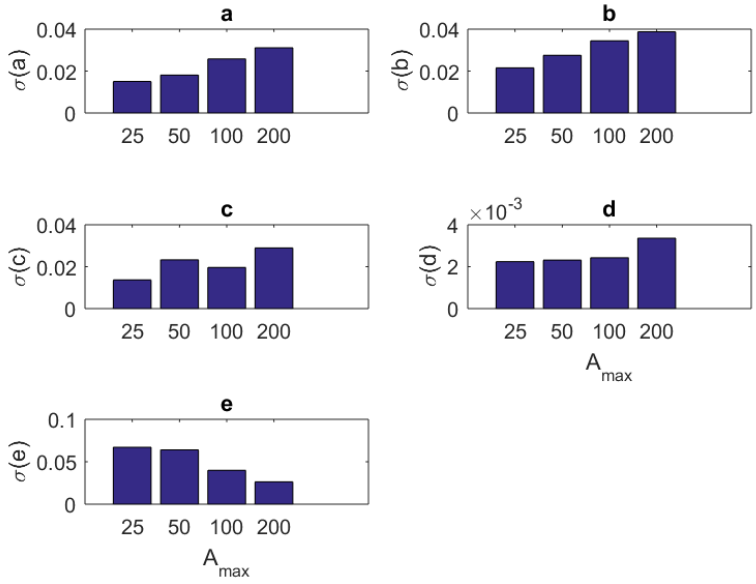

Figure 5.2: The variation of individual for (relative errors SD) of the estimates against varying stimulus amplitude parameter $A_{\max}$. Where $N_{it} = 100$, $N_U = 5$, and $f_0 = 333.3$ Hz. Except for parameter F, one cannot see an improvement with raising the stimulus amplitude. However, in general, the relative error levels remain small.

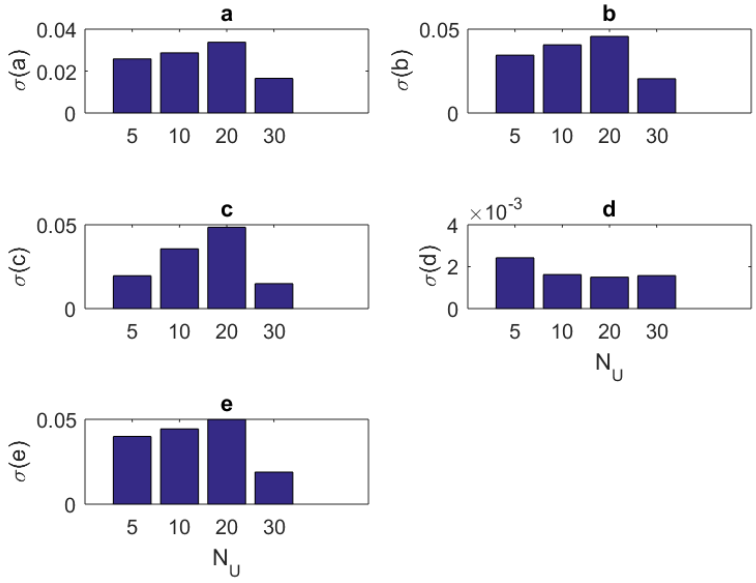

Figure 5.3: The variation of individual SD (relative errors) of the estimates against varying stimulus component size N_U. where $N_{it} = 100$, $A_{\max} = 100$, and $f_0 = 333.3$ Hz. Stimuli with small $N_U = 5$ or large $N_U = 30$ component size can be preferred. In general, relative error levels also stay smaller in this case.

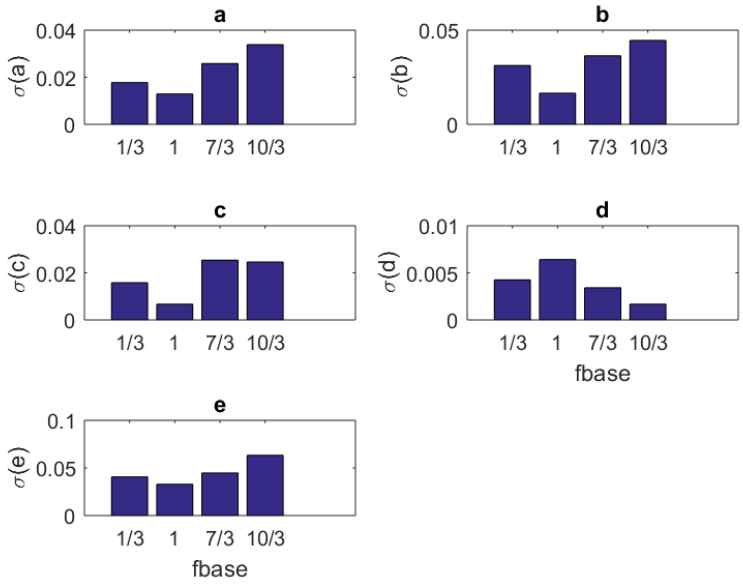

Figure 5.4: The variation of individual standard deviations (or relative errors) of the estimates against varying base frequency f_0. Other stimulus parameters are $N_{it} = 100$, $A_{\max} = 100$, and $N_U = 5$. The frequencies are in KHz. Although overall relative error levels are smaller, one can prefer a mid frequency range, e.g. $1 \leq f_0 \leq 7/3$ KHz

Thus, in its first column, the relative error of the case with $N_{it} = 50$ was computed against the case with $N_{it} = 25$. Similarly, the relative error of the case with $N_{it} = 100$ was computed against the case with $N_{it} = 50$, and so on. When we examine Table 5.10, we can observe that the relative errors (ER) of parameters $[a, b, c, d, F]$ reduce as the sample size increases (as k progresses). Although there seems a fluctuation of the relative error, the magnitude of this fluctuation tends to decrease. This is noted especially after the case with $N_{it} = 600$.

5.1.4 Statistical Testing of the Parameter Estimation with Realistic Data

To test the validity of the results of Section 5.1.3, one needs to perform a statistical comparison test. To achieve this goal, we performed a Kolmogorov–Smirnov test on the inter-spike intervals of the spike trains obtained from the H1 neuron measurement data and the simulated spike trains with one of the parameter sets $[a, b, c, d, F]$ in Table 5.9. As one set of measurement is not statistically adequate, we used superimposed spike sequences. As they were obtained from independent stimuli, their statistical

Table 5.9: The variation of estimated parameters a, b, c, d, F against increasing sample size N_{it} in the estimation using realistic stimulus/response data obtained from H1 neurons of blowfly neurons.

Case #	N_{it}	$\hat{a}$	$\hat{b}$	$\hat{c}$	$\hat{d}$	$\hat{F}$
1	25	255.7506	23.1953	344.3629	0.0000	185.6737
2	50	209.6757	21.3999	288.8835	0.0814	157.9571
3	100	233.4375	21.2668	266.9164	0.0492	154.7241
4	200	238.6861	21.1010	242.4651	0.0571	150.1093
5	300	244.5549	20.8891	239.7912	0.0777	145.6895
6	400	238.0263	20.1484	227.6343	0.1002	145.9515
7	500	220.6098	19.5167	212.1591	0.1091	142.7544
8	600	209.2398	18.9435	203.5418	0.1155	140.1229
9	700	208.3796	18.6725	200.2183	0.1180	138.9247
10	800	205.1722	18.6186	196.1978	0.1294	138.2120
11	900	206.8349	18.7251	195.6544	0.1247	137.1808
12	1000	204.2514	18.5038	192.3779	0.1250	135.9998
13	1100	201.7751	18.6313	191.4930	0.1164	136.7989
14	1200	199.1862	18.7457	190.4784	0.1237	136.2337
15	1300	196.8611	18.6375	190.3953	0.1201	135.1311
16	1400	198.3144	18.5702	190.7353	0.1230	135.3718
17	1500	196.1595	18.3109	189.0624	0.1306	134.3871
18	1600	192.2135	17.9623	185.5415	0.1447	133.7077
19	1700	190.5854	17.8516	183.7031	0.1508	133.3508
20	1800	190.7481	17.8419	184.6075	0.1495	133.5511
21	1900	192.3369	17.8900	185.2415	0.1473	133.6132
22	2000	194.9553	18.0284	185.7370	0.1495	133.5813
23	2100	198.5889	18.1381	187.4582	0.1452	134.3980
24	2200	200.3984	18.1539	188.0695	0.1366	134.8025
25	2300	201.9018	18.2673	188.5241	0.1356	134.8863
26	2400	201.6645	18.2587	187.8792	0.1357	135.2327

nature was not disturbed. As we did in the estimation experiment, we superimposed the spike sequences in the response segments of both realistic measurements and the simulated output from our model. After obtaining that, we performed a Kolmogorov–Smirnov test for the two samples (one is from realistic response and one is from the simulated response from our model). We applied different segment lengths and plotted the variation of the p-values. The tool used in the application was MATLAB's **kstest2(x1,x2)** routine (here, **x1** and **x2** are two samples from similar or dissimilar distributions). We used the parametric estimations from the last column in Table 5.9. One can see the relevant results in Figures 5.5–5.10. From those outcomes, one can note that the p-value starts crossing the $p = 0.05$ line after obtaining about 80 samples of measurement. This may be normal in the view of statistics, as these hypothesis testing algorithms require large numbers of samples to yield strong results.

Table 5.10: The relative error levels against the sample size parameter N_{it}. The errors were computed by evaluating the difference between the parameter values of the current case k and the previous case $k-1$ in Table 5.9. With increasing sample sizes, the estimates tend to have smaller fluctuations.

N_{it}	e_a	e_b	e_c	e_d	e_F
50	0.18016	0.07741	0.16111	Inf	0.14928
100	0.11333	0.00622	0.07604	0.39521	0.02047
200	0.02248	0.00779	0.09161	0.16078	0.02983
300	0.02459	0.01004	0.01103	0.35951	0.02944
400	0.02670	0.03546	0.05070	0.28976	0.00180
500	0.07317	0.03135	0.06798	0.08886	0.02191
600	0.05154	0.02937	0.04062	0.05941	0.01843
700	0.00411	0.01431	0.01633	0.02123	0.00855
800	0.01539	0.00288	0.02008	0.09665	0.00513
900	0.00810	0.00572	0.00277	0.03619	0.00746
1000	0.01249	0.01182	0.01675	0.00208	0.00861
1100	0.01212	0.00689	0.00460	0.06885	0.00588
1200	0.01283	0.00614	0.00530	0.06300	0.00413
1300	0.01167	0.00577	0.00044	0.02875	0.00809
1400	0.00738	0.00361	0.00179	0.02359	0.00178
1500	0.01087	0.01397	0.00877	0.06198	0.00727
1600	0.02012	0.01904	0.01862	0.10819	0.00505
1700	0.00847	0.00616	0.00991	0.04207	0.00267
1800	0.00085	0.00054	0.00492	0.00871	0.00150
1900	0.00833	0.00270	0.00343	0.01443	0.00047
2000	0.01361	0.00773	0.00267	0.01429	0.00024
2100	0.01864	0.00608	0.00927	0.02861	0.00611
2200	0.00911	0.00087	0.00326	0.05905	0.00301
2300	0.00750	0.00625	0.00242	0.00735	0.00062
2400	0.00118	0.00048	0.00342	0.00091	0.00257

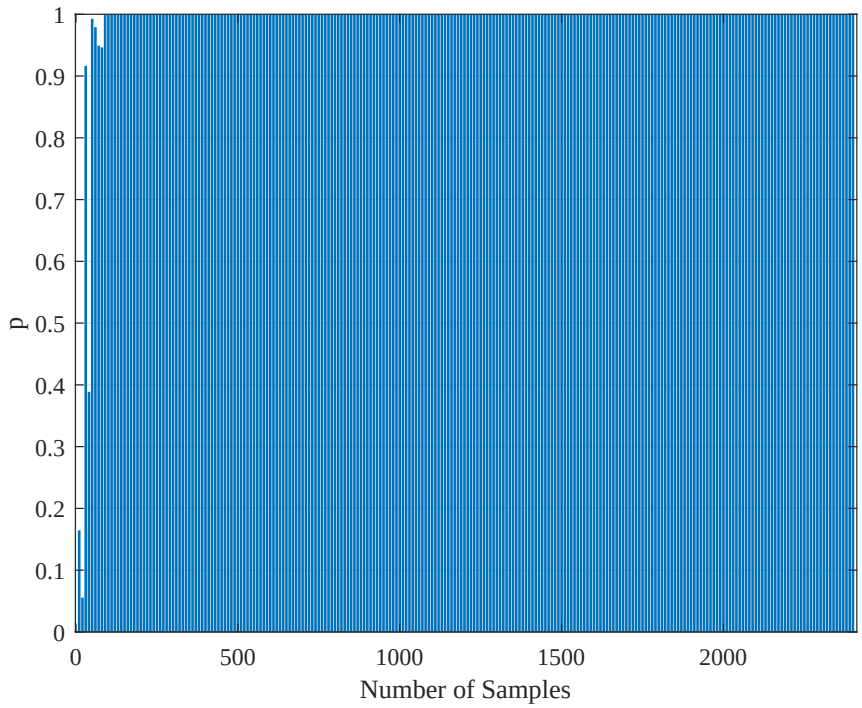

Figure 5.5: The variation of the Kolmogorov–Smirnov test p value with the number of samples N_{it} obtained from both measurements (simulation and realistic measurement). Here, the segment size is 500 ms.

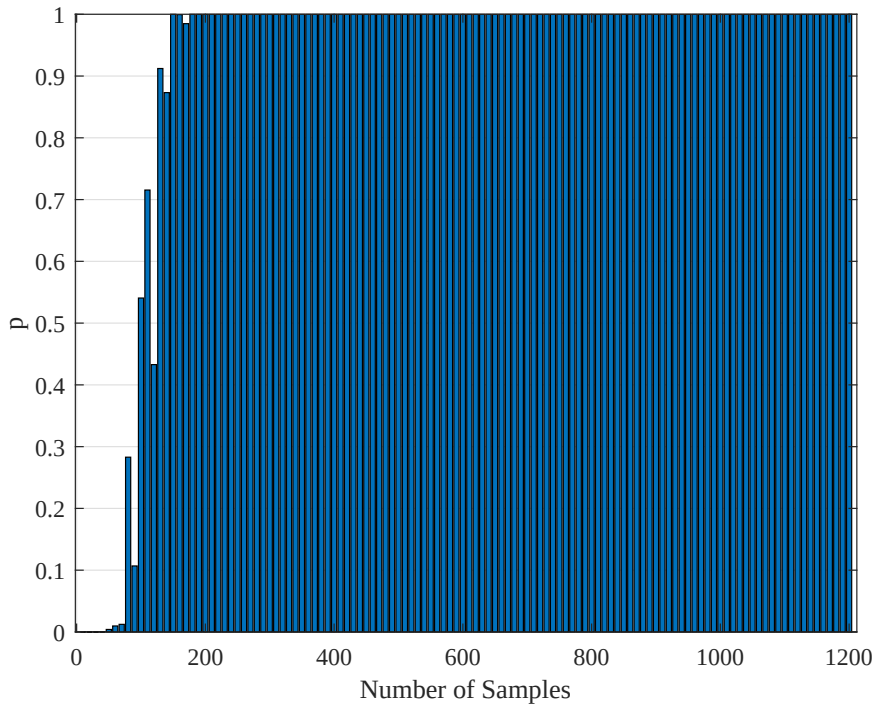

Figure 5.6: The variation of the Kolmogorov–Smirnov test p value with the number of samples N_{it} obtained from both measurements (simulation and realistic measurement). Here, the segment size is 1 s.

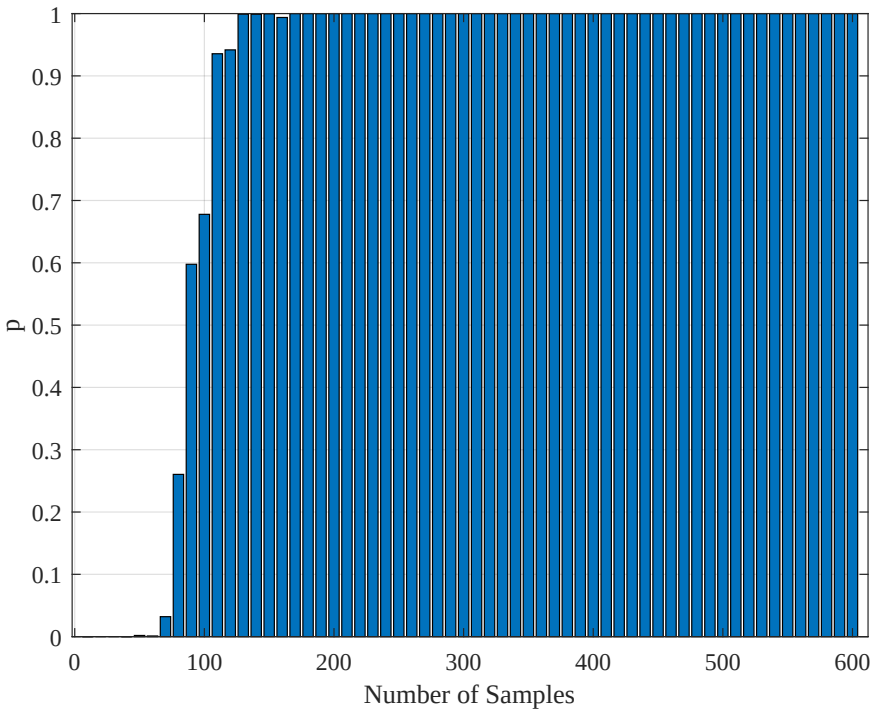

Figure 5.7: The variation of the Kolmogorov–Smirnov test p value with the number of samples N_{it} obtained from both measurements (simulation and realistic measurement). Here, the segment size is 2 s.

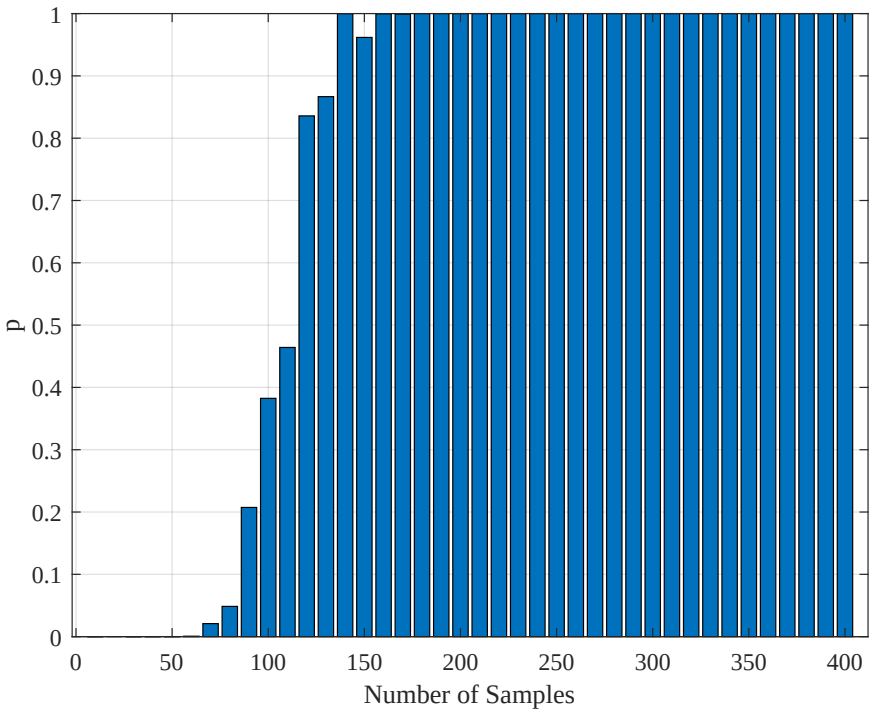

Figure 5.8: The variation of the Kolmogorov–Smirnov test p value with the number of samples N_{it} obtained from both measurements (simulation and realistic measurement). Here, the segment size is 3 s.

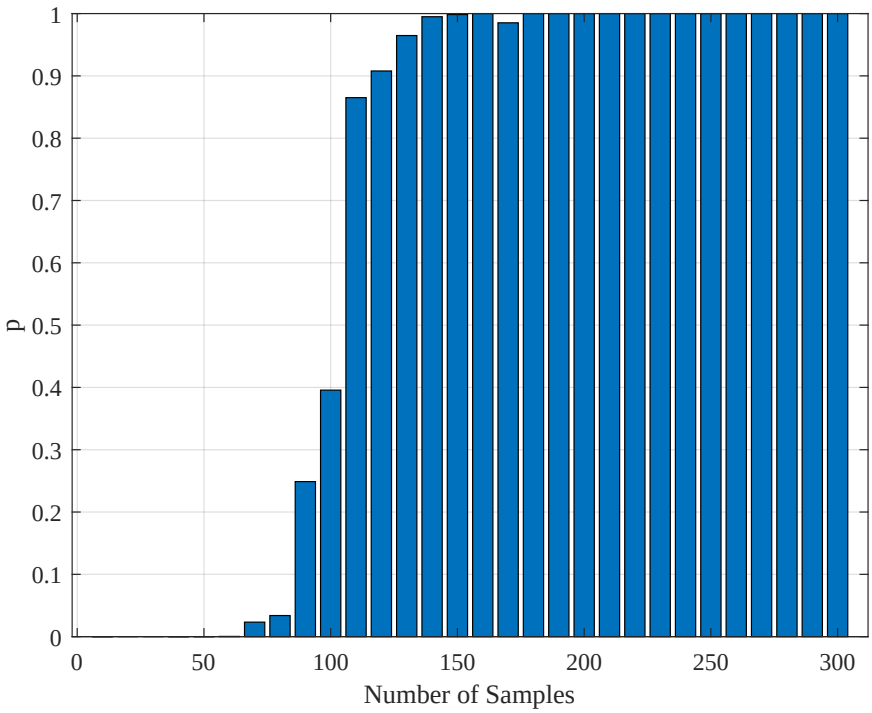

Figure 5.9: The variation of the Kolmogorov–Smirnov test p value with the number of samples N_{it} obtained from both measurements (simulation and realistic measurement). Here, the segment size is 4 s.

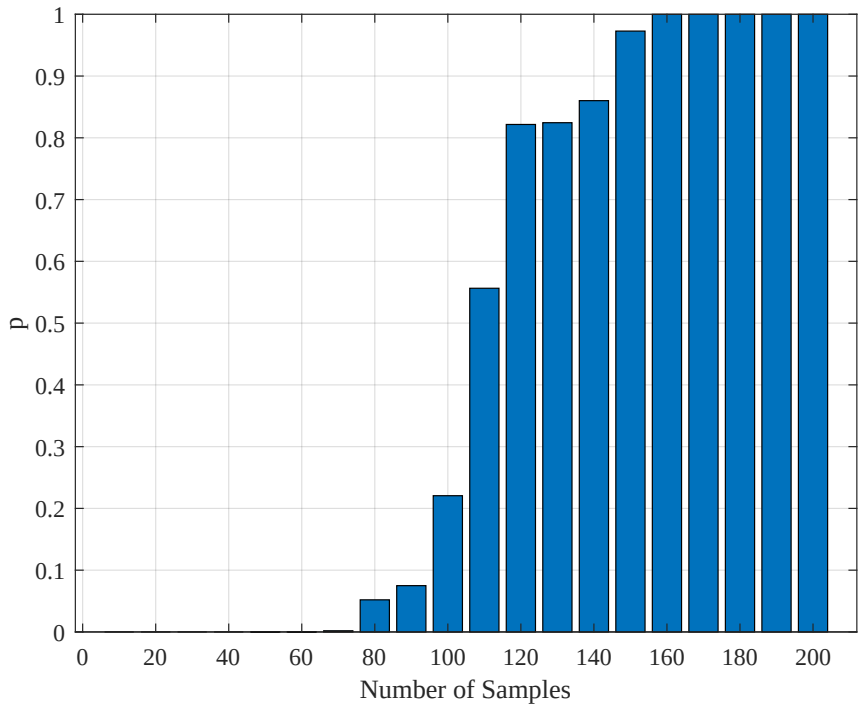

Figure 5.10: The variation of the Kolmogorov–Smirnov test p value with the number of samples N_{it} obtained from both measurements (simulation and realistic measurement). Here, the segment size is 6 s.

CHAPTER 6

CONCLUSION

In this paper, we present a theoretical and computational study aiming at the identification of the parameters of a single Fitzhugh–Nagumo model from stochastic discrete neural spiking data. To pursue this goal, we needed to modify the classical Fitzhugh–Nagumo model so that the output generates a firing rate instead of a membrane potential. We transformed the membrane potential information into that of a time dependent firing rate through a nonlinear map in sigmoidal form. The spiking data that are representative of an experimental application were obtained by simulating the Fitzhugh–Nagumo model and an Inhomogeneous Poisson process together. To assess the performance of the work, we repeated the simulations under different sample sizes (the number of repeated trials), stimulus component sizes, and stimulus base frequencies and amplitudes. The variation of mean estimated values and standard deviations are presented as results. The following concluding remarks can be made:

- The estimation algorithm showed a stable behavior for all examined conditions, as shown in Table 4.1.
- The results in Tables 5.1–5.4 show that the mean estimated values are closest to the true values of the parameters in Table 3.2 when $N_{it} = 100$, $N_U = 5$, $f_0 = 0.333$ KHz, and $A_{\max} = 25$.
- In general, the standard deviations of estimates present a decreasing behavior increasing sample size N_{it} (Figure 5.1). For parameters b and c, there is a slightly oscillating behavior in the standard deviation values (Figure 5.1b,c). The standard deviations when $N_{it} = 100$ are slightly larger than those of the case $N_{it} = 200$. The situation may be treated inferior to the results of others

studies (e.g., [67]). However, one should bear in mind that the model in [67] is a type of generic recurrent neural network and those are known to have universal approximation capabilities [68]. Thus, one should expect that the standard deviations of network weight estimates will have a better correlation to stimulus parameters when a generic model with a universal approximation capability is utilized for model fitting. In addition, the absolute standard deviations of the estimates in this research seem smaller. Thus, the overall results can be considered successful.

- For most of the parameters (a, b, c, d), the variation of standard deviations against the amplitude parameter $A_{\max}$ has a worsening behavior (Figure 5.2). The only exception is associated with the maximum firing rate parameter F. It has an improved standard deviation when the amplitude level $A_{\max}$ increases. Concerning the mean estimated values, changing the amplitude from $A_{\max} = 25$ to $A_{\max} = 200$ does not make a sensible variation. Thus, keeping $A_{\max} = 25$ seems a good choice.

- Standard deviations of the estimates showed a little improvement when one has a large number of stimulus components N_U (Figure 5.3). However, based on the mean estimated values, keeping it smaller together with the amplitude parameter $A_{\max}$ seems a viable choice.

- Concerning the stimulus base frequency f_0, it seems better to keep it in the lower side of the range ($0.333 \leq f_0 \leq 3.333$ KHz) applied in this research (i.e., $f_0 \leq 1$ KHz).

- For assessing the performance of our model when more realistic data and longer stimuli exist, we performed an estimation attempt using the data from a previous research [66]. We divided a 20 min recording into 2400 segments, the lengths of which equal 500 ms each. The stimulus was randomly generated and thus each segment was treated as an independent experiment. It appears that the estimates of the parameters have a tendency to converge to a final value, with the increasing sample size N_{it}. This can be understood from the relative errors in Table 5.10. The errors become smaller and fluctuations diminish as the sample size advances. As a result, our model can be used in modeling studies where

the computational features of the neural signal processing is important.

- The statistical Kolmogorov–Smirnov testing reveals that our modified Fitzhugh–Nagumo computational model can successfully describe the statistics stimulus/response relationship.

REFERENCES

[1] E. M. Izhikevich and R. FitzHugh, "Fitzhugh-nagumo model," *Scholarpedia*, vol. 1, no. 9, p. 1349, 2006.

[2] A. L. Hodgkin and A. F. Huxley, "A quantitative description of membrane current and its application to conduction and excitation in nerve," *The Journal of physiology*, vol. 117, no. 4, pp. 500–544, 1952.

[3] C. Morris and H. Lecar, "Voltage oscillations in the barnacle giant muscle fiber," *Biophysical journal*, vol. 35, no. 1, pp. 193–213, 1981.

[4] R. FitzHugh, "Impulses and physiological states in theoretical models of nerve membrane," *Biophysical journal*, vol. 1, no. 6, pp. 445–466, 1961.

[5] V. Booth, J. Rinzel, and O. Kiehn, "Compartmental model of vertebrate motoneurons for ca2+-dependent spiking and plateau potentials under pharmacological treatment," *Journal of Neurophysiology*, vol. 78, no. 6, pp. 3371–3385, 1997.

[6] V. Mante, R. A. Frazor, V. Bonin, W. S. Geisler, and M. Carandini, "Independence of luminance and contrast in natural scenes and in the early visual system," *Nature neuroscience*, vol. 8, no. 12, p. 1690, 2005.

[7] E. H. Adelson and J. R. Bergen, "Spatiotemporal energy models for the perception of motion," *Josa a*, vol. 2, no. 2, pp. 284–299, 1985.

[8] L. Buhry, S. Saighi, A. Giremus, E. Grivel, and S. Renaud, "Parameter estimation of the hodgkin-huxley model using metaheuristics: application to neuromimetic analog integrated circuits," in *2008 IEEE Biomedical Circuits and Systems Conference*, pp. 173–176, IEEE, 2008.

[9] J. Sun, B. Deng, X. Wei, C. Jia, J. Wang, and J. Zhao, "Parameter estimation in hodgkin-huxley model with adaptive method," in *2011 4th International Conference on Biomedical Engineering and Informatics (BMEI)*, vol. 4, pp. 1853–1857, IEEE, 2011.

[10] I. Tyukin, E. Steur, H. Nijmeijer, D. Fairhurst, I. Song, A. Semyanov, and C. V. LEEUWEN, "State and parameter estimation for canonic models of neural oscillators," *International journal of neural systems*, vol. 20, no. 03, pp. 193–207, 2010.

[11] D. Fairhurst, I. Tyukin, H. Nijmeijer, and C. van Leeuwen, "Observers for canonic models of neural oscillators," *Mathematical Modelling of Natural Phenomena*, vol. 5, no. 2, pp. 146–184, 2010.

[12] B. Deng, J. Wang, and Y. Che, "A combined method to estimate parameters of neuron from a heavily noise-corrupted time series of active potential," *Chaos: An Interdisciplinary Journal of Nonlinear Science*, vol. 19, no. 1, p. 015105, 2009.

[13] S. J. Julier and J. K. Uhlmann, "Unscented filtering and nonlinear estimation," *Proceedings of the IEEE*, vol. 92, no. 3, pp. 401–422, 2004.

[14] I. Tokuda, U. Parlitz, L. Illing, M. Kennel, and H. Abarbanel, "Parameter estimation for neuron models," in *AIP Conference Proceedings*, vol. 676, pp. 251–256, American Institute of Physics, 2003.

[15] U. Parlitz, L. Junge, and L. Kocarev, "Synchronization-based parameter estimation from time series," *Physical Review E*, vol. 54, no. 6, p. 6253, 1996.

[16] Y. Che, L.-H. Geng, C. Han, S. Cui, and J. Wang, "Parameter estimation of the fitzhugh-nagumo model using noisy measurements for membrane potential," *Chaos: An Interdisciplinary Journal of Nonlinear Science*, vol. 22, no. 2, p. 023139, 2012.

[17] R. T. Faghih, K. Savla, M. A. Dahleh, and E. N. Brown, "Broad range of neural dynamics from a time-varying fitzhugh–nagumo model and its spiking threshold estimation," *IEEE transactions on biomedical engineering*, vol. 59, no. 3, pp. 816–823, 2011.

[18] I. Daubechies, *Ten lectures on wavelets*, vol. 61. Siam, 1992.

[19] J. O. Ramsay, G. Hooker, D. Campbell, and J. Cao, "Parameter estimation for differential equations: a generalized smoothing approach," *Journal of the Royal Statistical Society: Series B (Statistical Methodology)*, vol. 69, no. 5, pp. 741–796, 2007.

[20] H. Liang and H. Wu, "Parameter estimation for differential equation models using a framework of measurement error in regression models," *Journal of the American Statistical Association*, vol. 103, no. 484, pp. 1570–1583, 2008.

[21] A. Borst and F. E. Theunissen, "Information theory and neural coding," *Nature neuroscience*, vol. 2, no. 11, p. 947, 1999.

[22] B. Hassenstein and W. Reichardt, "Systemtheoretische analyse der zeit-, reihenfolgen-und vorzeichenauswertung bei der bewegungsperzeption des rüsselkäfers chlorophanus," *Zeitschrift für Naturforschung B*, vol. 11, no. 9-10, pp. 513–524, 1956.

[23] A. V. Herz, T. Gollisch, C. K. Machens, and D. Jaeger, "Modeling single-neuron dynamics and computations: a balance of detail and abstraction," *science*, vol. 314, no. 5796, pp. 80–85, 2006.

[24] J. Ma and J. Tang, "A review for dynamics in neuron and neuronal network," *Nonlinear Dynamics*, vol. 89, no. 3, pp. 1569–1578, 2017.

[25] J. A. White, J. T. Rubinstein, and A. R. Kay, "Channel noise in neurons," *Trends in neurosciences*, vol. 23, no. 3, pp. 131–137, 2000.

[26] M. Lv, C. Wang, G. Ren, J. Ma, and X. Song, "Model of electrical activity in a neuron under magnetic flow effect," *Nonlinear Dynamics*, vol. 85, no. 3, pp. 1479–1490, 2016.

[27] F. Wu, C. Wang, Y. Xu, and J. Ma, "Model of electrical activity in cardiac tissue under electromagnetic induction," *Scientific reports*, vol. 6, no. 1, p. 28, 2016.

[28] Y. Wang, J. Ma, Y. Xu, F. Wu, and P. Zhou, "The electrical activity of neurons subject to electromagnetic induction and gaussian white noise," *International Journal of Bifurcation and Chaos*, vol. 27, no. 02, p. 1750030, 2017.

[29] F. Zhan and S. Liu, "Response of electrical activity in an improved neuron model under electromagnetic radiation and noise," *Frontiers in computational neuroscience*, vol. 11, p. 107, 2017.

[30] F. Wu, C. Wang, W. Jin, and J. Ma, "Dynamical responses in a new neuron model subjected to electromagnetic induction and phase noise," *Physica A: Statistical Mechanics and its Applications*, vol. 469, pp. 81–88, 2017.

[31] C. DiMattina and K. Zhang, "Adaptive stimulus optimization for sensory systems neuroscience," *Frontiers in neural circuits*, vol. 7, p. 101, 2013.

[32] C. DiMattina and K. Zhang, "How to modify a neural network gradually without changing its input-output functionality," *Neural computation*, vol. 22, no. 1, pp. 1–47, 2010.

[33] R. O. Doruk and K. Zhang, "Fitting of dynamic recurrent neural network models to sensory stimulus-response data," *Journal of biological physics*, vol. 44, no. 3, pp. 449–469, 2018.

[34] J. Huguenard and D. A. McCormick, *Electrophysiology of the neuron: an interactive tutorial*. No. 577.25 SHE, 1994.

[35] S. Ianigro and O. Bown, "Exploring continuous time recurrent neural networks through novelty search," in *Proceedings of the international conference on new interfaces for musical expression. Blacksburg. Virginia Tech*, pp. 108–113, 2018.

[36] C. Wang, S. Guo, Y. Xu, J. Ma, J. Tang, F. Alzahrani, and A. Hobiny, "Formation of autapse connected to neuron and its biological function," *Complexity*, vol. 2017, 2017.

[37] S. Guo, C. Wang, J. Ma, and W. Jin, "Transmission of blocked electric pulses in a cable neuron model by using an electric field," *Neurocomputing*, vol. 216, pp. 627–637, 2016.

[38] Y. Xu, H. Ying, Y. Jia, J. Ma, and T. Hayat, "Autaptic regulation of electrical activities in neuron under electromagnetic induction," *Scientific reports*, vol. 7, p. 43452, 2017.

[39] B. Jia, "Negative feedback mediated by fast inhibitory autapse enhances neuronal oscillations near a hopf bifurcation point," *International Journal of Bifurcation and Chaos*, vol. 28, no. 02, p. 1850030, 2018.

[40] P. Dayan, L. F. Abbott, *et al.*, *Theoretical neuroscience*, vol. 806. Cambridge, MA: MIT Press, 2001.

[41] H. C. Tuckwell, *Introduction to theoretical neurobiology: volume 2, nonlinear and stochastic theories*, vol. 8. Cambridge University Press, 1988.

[42] M. N. Shadlen and W. T. Newsome, "Noise, neural codes and cortical organization," *Current opinion in neurobiology*, vol. 4, no. 4, pp. 569–579, 1994.

[43] B. Pesaran, "Neural signal processing: quantitative analysis of neural activity," in *Short course III, presented at 2008 Society for Neuroscience Annual Meeting (Mitra PP, ed)*, pp. 1–12, 2008.

[44] J. Carrera and S. P. Neuman, "Estimation of aquifer parameters under transient and steady state conditions: 1. maximum likelihood method incorporating prior information," *Water Resources Research*, vol. 22, no. 2, pp. 199–210, 1986.

[45] I. J. Myung, "Tutorial on maximum likelihood estimation," *Journal of mathematical Psychology*, vol. 47, no. 1, pp. 90–100, 2003.

[46] S. Kollias and D. Anastassiou, "An adaptive least squares algorithm for the efficient training of artificial neural networks," *IEEE Transactions on Circuits and Systems*, vol. 36, no. 8, pp. 1092–1101, 1989.

[47] C.-N. Wang, J. Ma, and W.-Y. Jin, "Identification of parameters with different orders of magnitude in chaotic systems," *Dynamical Systems*, vol. 27, no. 2, pp. 253–270, 2012.

[48] E. P. Lynch and C. J. Houghton, "Parameter estimation of neuron models using in-vitro and in-vivo electrophysiological data," *Frontiers in neuroinformatics*, vol. 9, p. 10, 2015.

[49] T. Kreuz, D. Chicharro, C. Houghton, R. G. Andrzejak, and F. Mormann, "Monitoring spike train synchrony," *Journal of neurophysiology*, vol. 109, no. 5, pp. 1457–1472, 2012.

[50] M. v. Rossum, "A novel spike distance," *Neural computation*, vol. 13, no. 4, pp. 751–763, 2001.

[51] M. Nucci and P. Clarkson, "The nonclassical method is more general than the direct method for symmetry reductions. an example of the fitzhugh-nagumo equation," *Physics Letters A*, vol. 164, no. 1, pp. 49–56, 1992.

[52] R. Ö. DORUK, "Neuron modeling: estimating the parameters of a neuron model from neural spiking data," *Turkish Journal of Electrical Engineering & Computer Sciences*, vol. 26, no. 5, pp. 2301–2314, 2018.

[53] D. Heeger, "Poisson model of spike generation," *Handout, University of Standford*, vol. 5, pp. 1–13, 2000.

[54] J. L. Hindmarsh and R. Rose, "A model of neuronal bursting using three coupled first order differential equations," *Proceedings of the Royal society of London. Series B. Biological sciences*, vol. 221, no. 1222, pp. 87–102, 1984.

[55] R. FitzHugh, "Mathematical models of excitation and propagation in nerve," *Biological engineering*, pp. 1–85, 1969.

[56] J. Nagumo, S. Arimoto, and S. Yoshizawa, "An active pulse transmission line simulating nerve axon," *Proceedings of the IRE*, vol. 50, no. 10, pp. 2061–2070, 1962.

[57] E. T. Rolls, A. Treves, and E. T. Rolls, *Neural networks and brain function*, vol. 572. Oxford university press Oxford, 1998.

[58] A. Kemp, "Poisson processes," *Bulletin of the London Mathematical Society*, vol. 26, no. 6, pp. 612–614, 1994.

[59] Y. A. Kutoyants, "Nonparametric estimation of intensity function of inhomogeneous poisson process.," *PROB. CONTROL. INFO. THEORY.*, vol. 13, no. 4, pp. 253–258, 1984.

[60] U. T. Eden, "Point process models for neural spike trains," *Neural Signal Processing: Quantitative Analysis of Neural Activity*, pp. 45–51, 2008.

[61] E. N. Brown, R. Barbieri, V. Ventura, R. E. Kass, and L. M. Frank, "The time-rescaling theorem and its application to neural spike train data analysis," *Neural computation*, vol. 14, no. 2, pp. 325–346, 2002.

[62] R. Ö. DORUK and H. IHNISH, "Bifurcation control of fitzhugh-nagumo models," *Süleyman Demirel Üniversitesi Fen Bilimleri Enstitüsü Dergisi*, vol. 22, pp. 375–391.

[63] G. Czanner, U. T. Eden, S. Wirth, M. Yanike, W. A. Suzuki, and E. N. Brown, "Analysis of between-trial and within-trial neural spiking dynamics," *Journal of neurophysiology*, vol. 99, no. 5, pp. 2672–2693, 2008.

[64] P. W. Lewis and G. S. Shedler, "Simulation of nonhomogeneous poisson processes by thinning," *Naval research logistics quarterly*, vol. 26, no. 3, pp. 403–413, 1979.

[65] R. W. Klein and S. D. Roberts, "A time-varying poisson arrival process generator," *Simulation*, vol. 43, no. 4, pp. 193–195, 1984.

[66] R. de Ruyter and W. Bialek, "Timing and counting precision in the blowfly visual system," in *Models of Neural Networks IV*, pp. 313–371, Springer, 2002.

[67] R. O. Doruk and K. Zhang, "Fitting of dynamic recurrent neural network models to sensory stimulus-response data," *J Biol Phys*, vol. 44, pp. 449–469, jun 2018.

[68] A. M. Schäfer and H. G. Zimmermann, "Recurrent neural networks are universal approximators," in *International Conference on Artificial Neural Networks*, pp. 632–640, Springer, 2006.

APPENDIX A

MATLAB CODES

A.1 Program 1

The following are a MATLAB codes.

```
%At first try with Nita=10, 25, 50, 100, 200, 400.
%Set Amax=100, fbase and Nu are fine for the first attempt.
clc
clear
close all
% distcomp.feature( 'LocalUseMpiexec', false);
format long g
% parpool(24)"
Topt=30; % This should be same with the OED part.
         %You can take it from its saved mat file.
         %Normally it is 1 seconds
dt=1e-2;
Nopt=Topt/dt+1;
ta=0:dt:Topt;
Nita=100; % Number of repeated simulations.
          % Increasing simulations will increase the statistical
          % efficiency of estimation. The variance of estimation approaches
          % Cramer Rao bound when sample size approaches infinity.

% The true parameters
```

```
a = 0.08;
b = 0.056;
c = 0.064;
d=0.3333;
F = 100;

tht=[a b c d F]';

Amax=100; % The effect of amplitude parameter will be
          % investigated by changing this parameter.

fbase=10/Topt; % The effect of base frequency
               % parameter will be investigated by
               % changing this parameter.
Nu=30; % The effect of stimulus component size will be
       % investigated by changing this parameter.
wbase=2*pi*fbase;
WE=wbase*(1:Nu)';
AE=Amax.*ones(Nu,1);
lbp=zeros(length(tht),1);
ubp=2*tht;
for is=1:20
for oi=1:Nita
PE=unifrnd(-pi,pi,Nu,1);
v=0;
w=0;
for i=1:Nopt
t=ta(i);
u=sum(AE.*cos(WE.*t+PE));
v = v + dt*(v - (d)*v.^3 - w + u);
w = w + dt*(c * v + a - b.*w);
re=F/(1+exp(-v));
```

```
rea(i)=re;
end
rta=rea*dt;
uaar=unifrnd(0,1,1,Nopt);
shi=rta>uaar;
shinz=find(shi);
Tspks=ta(shinz);
uspks(oi).spks=Tspks';
uspks(oi).A=AE;
uspks(oi).P=PE;
uspks(oi).W=WE;
end
Nin=14;
sa=num2str(Amax);
sw=num2str(wbase);
sn=num2str(Nita);
snu=num2str(Nu);
fname=strcat('results_','nit_',sn,'_amax_',sa,
             '_wbase_',sw,'_nu_',snu,'.txt');
for k=1:Nin;
th0=unifrnd(lbp,ubp);
foptions=optimset('Algorithm','interior-point', 'Diagnostics','on',
                  'Display','iter', 'GradObj', 'off','Hessian','off',
                  'DerivativeCheck',
                  'off','TolFun',1e-6,'TolX',eps,
                  'TolCon',1e-6,
                  'MaxFunEvals',30000,'FunValCheck',
                  'off','MaxIter',500);
[theta,fvalp,exitflagp,outputp,lambdap,gradp,hessianp]
= fmincon(@(th)jhujed_obj(th,uspks,Topt,dt,Nita)
,th0,[],[],[],[],lbp,ubp,[],foptions);
fid=fopen(fname,'a+');
fprintf(fid,'%d %d %d %f %f | %f %f %f %f %f | %f %f %d %d\n',
```

```
is,k,exitflagp,fvalp,norm(gradp),theta',Amax,wbase,Nita,Nu);
fclose(fid);
end
end
% delete(gcp)
```

A.2 Program 2

```
function [J] = jhujed_obj(theta,uspks,Topt,dt,Nita)
a=theta(1);
b=theta(2);
c=theta(3);
d=theta(4);
F=theta(5);

Nopt=Topt/dt+1;
ta=0:dt:Topt;
rea=zeros(1,Nopt);
llkl=zeros(1,Nita);

for oi=1:Nita
Tspks=uspks(oi).spks;
AE=uspks(oi).A;
WE=uspks(oi).W;
PE=uspks(oi).P;
v=0;
w=0;
rei=0;
for i=1:Nopt
t=ta(i);
u=sum(AE.*cos(WE.*t+PE));
% ge=Fmaxe/(exp(ae*(vce - ve)) + 1);
```

```
% gev=(Fmaxe*ae*exp(ae*(vce - ve)))/(exp(ae*(vce - ve)) + 1)^2;
% gevv=(2*Fmaxe*ae^2*exp(2*ae*(vce - ve)))/
% (exp(ae*(vce - ve)) + 1)^3 - (Fmaxe*ae^2*exp(ae*(vce - ve)))/
% (exp(ae*(vce - % ve)) + 1)^2;
% gi=Fmaxi/(exp(ai*(vci - vi)) + 1);
% giv=(Fmaxi*ai*exp(ai*(vci - vi)))/(exp(ai*(vci - vi)) + 1)^2;
% givv=(2*Fmaxi*ai^2*exp(2*ai*(vci - vi)))/
% (exp(ai*(vci - vi)) + 1)^3 - (Fmaxi*ai^2*exp(ai*(vci - vi)))/
% (exp(ai*(vci - vi)) + 1)^2;
% vedot=be*(-ve+ge*wee-gi*wei+we*u);
% vidot=bi*(-vi-gi*wii+ge*wie+wi*u);
v = v + dt*(v - (d)*v.^3 - w + u);
w = w + dt*(c * v + a - b.*w);
re=F/(1+exp(-v));
rea(i)=re;
rei=rei+re*dt;
end
reas=interp1(ta,rea,Tspks);
lreas=log(reas);
sreas=sum(lreas);
llkl(oi)=-rei+sreas; % log likelihood value
end
J=-sum(llkl); % log likelihood is negated!!.
              % fmincon will minimize its objective bu
              % t putting a minus sign will reverse the
              % operation fmincon minimizes -J but J is
              % being maximized.
```